

*The origin of tree-ring reconstructed summer cooling in Northern Europe
during the 18th century eruption of Laki*

Julie Edwards (University of Arizona, julieedwards@email.arizona.edu), Kevin J. Anchukaitis (University of Arizona, kanchukaitis@arizona.edu), Björn E. Gunnarson (Stockholm University, bjorn.gunnarson@natgeo.su.se), Charlotte Pearson (University of Arizona, c.pearson@ltrr.arizona.edu), Kristina Seftigen (University of Gothenburg, Swiss Federal Institute for Forest Snow and Landscape Research WSL, kristina.seftigen@gvc.gu.se), Georg von Arx (Swiss Federal Institute for Forest Snow and Landscape Research WSL, Oeschger Centre for Climate Change Research, University of Bern, georg.vonarx@wsl.ch), Hans W. Linderholm (University of Gothenburg, hansl@gvc.gu.se)

This manuscript is a non-peer reviewed preprint that has been submitted for publication in *Paleoceanography and Paleoclimatology*. Please note that this manuscript has not been accepted for publication and subsequent versions may have different content. If accepted, the final version of this manuscript will be available via the “Peer-Reviewed Publication DOI” link. We welcome feedback - please feel free to contact Julie Edwards regarding the manuscript.

¹ **The origin of tree-ring reconstructed summer cooling**
² **in Northern Europe during the 18th century eruption**
³ **of Laki**

Julie Edwards^{1,2}, Kevin J. Anchukaitis^{1,2}, Björn E. Gunnarson³, Charlotte

Pearson², Kristina Seftigen^{4,5}, Georg von Arx^{5,6}, Hans W. Linderholm⁴

Corresponding author: Julie Edwards, julieedwards@email.arizona.edu

¹School of Geography, Development, and
Environment, University of Arizona,
Tucson, AZ

²Laboratory of Tree-Ring Research,
University of Arizona, Tucson, AZ

³Department of Physical Geography,
Stockholm University, Sweden

⁴Department of Earth Sciences, University
of Gothenburg, Gothenburg, Sweden

⁵Swiss Federal Institute for Forest Snow
and Landscape Research WSL, Birmensdorf
Switzerland

⁶Oeschger Centre for Climate Change
Research, University of Bern, Bern,
Switzerland

4 **Abstract.** Basaltic fissure eruptions, which are characteristic of Icelandic
5 volcanism, are extremely hazardous due to the large quantities of gases and
6 aerosols they release into the atmosphere. The 1783–1784 CE Laki eruption
7 was one of the most significant high-latitude eruptions in the last millennium
8 and had substantial environmental and climatic impacts. Contemporary ob-
9 servations recorded the presence of a sulfuric haze over Iceland and Europe,
10 which caused famine from vegetation damage and resulted in a high occur-
11 rence of respiratory illnesses and related mortality. Historical records in north-
12 ern Europe show that the summer of 1783 was anomalously warm, but re-
13 gional tree-ring maximum latewood density (MXD) data from that year are
14 low and lead to erroneously colder reconstructed summer temperatures. Here
15 we measure wood anatomical characteristics of Scots pine (*Pinus sylvestris*)
16 from Jämtland, Sweden in order to identify the cause of this discrepancy. We
17 show that the presence of intra-annual density fluctuations in the majority
18 of 1783 growth rings, a sudden reduction in lumen and cell wall area, and
19 the measurement resolution of traditional x-ray densitometry lead to the ob-
20 served reduced annual MXD value. Multiple independent lines of evidence
21 suggest these anatomical anomalies were most likely the result of direct acidic
22 damage to trees in Northern Europe. The common relationship between sum-
23 mer temperature and MXD can be disrupted by acidic haze damage to trees.
24 Our study also demonstrates that quantitative wood anatomy offers a high
25 resolution approach to identifying anomalous years and extreme events in
26 the tree-ring record.

1. Introduction

27 More than 800 million people live within 100 km of an active volcano and may therefore
28 potentially be exposed to health and environmental hazards from eruptions [*Hansell and*
29 *Oppenheimer*, 2004; *Brown et al.*, 2015]. Basaltic fissure eruptions, which are charac-
30 teristic of Icelandic volcanism, are particularly hazardous due to the large quantities of
31 gases and aerosols released into the atmosphere [*Thordarson and Larsen*, 2007; *Carlsen*
32 *et al.*, 2021] and simulations of the health consequences of volcanic air pollution confirm
33 that future events pose a considerable risk to the UK and Europe [*Schmidt et al.*, 2011;
34 *Schmidt*, 2015; *Carlsen et al.*, 2021; *Dawson et al.*, 2021]. Icelandic eruption aerosols may
35 also cause a decrease in temperatures or reduction of incoming solar radiation, causing
36 widespread reductions in agricultural yields, as was observed during the 939 – 940 CE
37 Eldgjá eruption [*Oppenheimer et al.*, 2018]. More recently, even the comparatively small
38 2010 CE Eyjafjallajökull and the 2011 CE Grímsvötn eruptions impeded air travel and
39 caused economic disruption across Europe and the North Atlantic [*Budd et al.*, 2011;
40 *Gudmundsson et al.*, 2012; *Oppenheimer*, 2015; *Schmidt*, 2015]. These two modern erup-
41 tions and the 2014 CE – 2015 CE Holuhraun eruption also caused detrimental respiratory
42 health effects [*Carlsen et al.*, 2012; *Damby et al.*, 2017; *Carlsen et al.*, 2021]. Over the
43 entirety of the Common Era however, the 939 – 940 CE Eldgjá and 1783 – 1784 CE Laki
44 (Lakagígar) eruptions have thus far had the most significant environmental and climatic
45 impacts. The Laki eruption was one of the largest, in terms of the mass of SO₂ emitted,
46 high-latitude eruptions of the last millennium [*Thordarson and Larsen*, 2007; *Sigl et al.*,
47 2015] and among the most deadly of the last 400 years [*Auker et al.*, 2013]. The study of

48 previous Common Era eruptions provides perspective on the potential hazards and future
49 impacts of Icelandic volcanic eruptions.

50 The 1783–1784 Laki eruption is particularly interesting because it coincided with a pe-
51 riod of extreme and unusual weather and atmospheric phenomena across Europe. The
52 Laki eruption sequence began in June 8, 1783 and did not end until February 7, 1784,
53 emitting an estimated 122 megatons SO_2 into the atmosphere [*Thordarson and Self*,
54 2003]. Contemporary observations establish both the occurrence of a “haze” across Eu-
55 rope and an abnormal heat wave in Western and Central Europe during the summer of
56 1783 [*Franklin*, 1785; *Thordarson and Self*, 1993; *Grattan and Charman*, 1994; *Stothers*,
57 1996; *Grattan and Pyatt*, 1999; *Grattan and Sadler*, 1999; *Thordarson and Self*, 2003;
58 *Luterbacher et al.*, 2004]. This opaque dry haze in the lower troposphere, comprised
59 mostly of sulfuric acid (H_2SO_4), was observed across most of Europe by June 26, and
60 while the last known appearance of this haze is ambiguous it is likely to have been late in
61 October of 1783 [*Thordarson and Self*, 2003; *Oman et al.*, 2006]. Modeling experiments
62 show high surface sulfate aerosol concentrations averaged over the longitude band from
63 24.48°W (Iceland) to 5.68°E (Western Europe) centered around 65°N throughout the sum-
64 mer of that year [*Chenet et al.*, 2005]. The warm summer temperatures were intensified
65 by anomalously high pressure and atmospheric blocking over Europe, which would have
66 also contributed to a more persistent haze [*Thordarson and Self*, 2003; *Zambri et al.*,
67 2019a]. Retrospective studies have shown that the synoptic atmospheric configuration at
68 the time of the eruption could be considered the worst-case scenario in terms of bringing
69 volcanic pollution to Europe [*Dawson et al.*, 2021]. The haze, also referred to as a “dry
70 fog”, lead to widespread respiratory illnesses across Europe [*Durand and Grattan*, 1999;

71 *Grattan et al.*, 2003; *Witham and Oppenheimer*, 2004]. A Laki-like eruption today would
72 be a severe health and environmental hazard across Europe [*Schmidt et al.*, 2011; *Schmidt*,
73 2015; *Sonnek et al.*, 2017].

74 While summer cooling due to the reduction of incoming solar radiation is the expected
75 and frequently observed climate response to volcanic eruptions [*Robock*, 2000; *Timm-*
76 *reck*, 2012], early instrumental and documentary historical records actually show that
77 the summer of 1783 was abnormally warm throughout much of Europe, including Swe-
78 den [*Thordarson and Self*, 2003; *Luterbacher et al.*, 2004]. This time frame coincides
79 with when models show peak sulfate loading in the upper troposphere/lower stratosphere
80 [*Oman et al.*, 2006; *Zambri et al.*, 2019b]. The summer heatwave has been associated with
81 the presence of a high pressure air mass, and written records associate the hottest days
82 of this period with the thickest occurrences of the Laki haze [*Thordarson and Self*, 2003].
83 It has been suggested that the haze may also have played a role in exacerbating localized
84 warming [*Grattan and Sadler*, 1999]. Tree-ring data are often used to reconstruct the cli-
85 mate consequences of past volcanic eruptions and maximum latewood density (MXD) is
86 considered to be the most accurate metric for quantifying volcanic climate signals [*Frank*
87 *et al.*, 2007; *D'Arrigo et al.*, 2013; *Esper et al.*, 2015; *Anchukaitis et al.*, 2017; *Esper et al.*,
88 2018; *Björklund et al.*, 2019]. Contrary to the historical record however, temperature
89 reconstructions that use MXD indicate widespread cooling over much of Europe in the
90 summer of 1783 [*Tingley and Huybers*, 2013; *Hakim et al.*, 2016; *Luterbacher et al.*, 2016;
91 *Anchukaitis et al.*, 2017; *Guillet et al.*, 2017; *Tardif et al.*, 2019; *Edwards et al.*, 2021]. As
92 an example, the *Luterbacher et al.* [2004] reconstruction used predominantly historical,
93 documentary, and early instrumental data to estimate past temperatures and thus shows

94 the warming over much of northern Europe, including Sweden, in 1783. However, the
95 more recent *Luterbacher et al.* [2016] reconstruction uses predominantly tree-ring data
96 over this region, and shows cooling in 1783 (Figure 1). Previous authors have speculated
97 this inconsistency – which is seen in most tree-ring reconstructions [*Edwards et al.*, 2021]
98 – might be the direct result of the volcanic eruption on European tree growth [*Schove*,
99 1954; *Briffa et al.*, 1988; *Jones et al.*, 1995]. While weather conditions across Europe were
100 variable throughout the summer of 1783 (it was for instance indeed unusually cold in
101 Iceland) [*Thordarson and Self*, 2003], here we are specifically concerned with the discrep-
102 ancies between the tree-ring reconstructed cooling and the observed warming recorded
103 over Northern Europe. In this study we use new quantitative wood anatomy analyses,
104 historical temperature data, and existing tree-ring carbon isotope data to investigate the
105 origin of this discrepancy between the tree-ring temperature proxy data and 18th century
106 weather observations. By investigating this difference, we seek to more fully understand
107 the European environmental impacts of the eruption, provide information on the poten-
108 tial biological effects of future Icelandic fissure eruptions, and address the paleoclimate
109 implications of the direct impacts of extreme events on tree-ring proxy data.

2. Methods and Data

2.1. Quantitative Wood Anatomy

110 Both living and preserved dead samples of Scots pine (*Pinus sylvestris*) were collected
111 just east of the Scandinavian Mountains in Jämtland (Sweden) to produce an updated C-
112 Scan (central Scandinavia) reconstruction (63.30°N , 13.25°E; Figure 2), herein identified
113 as CSCAN2019 [*Zhang et al.*, 2016; *Linderholm and Gunnarson*, 2019]. Jämtland is one
114 of several Fennoscandian and northwestern Siberia tree-ring density chronologies, includ-

115 ing also the Polar Urals, Kola Peninsula, Yamal, and Forfjorddalen, that contribute to
116 reconstructed cold temperature anomalies across northern Europe region in 1783 [*Wilson*
117 *et al.*, 2016; *Anchukaitis et al.*, 2017]. Most importantly, Jämtland is also relatively close
118 to several 18th century historical climate data records that can be used for comparison
119 with the proxy record (see Section 2.2). There is also an existing tree-ring carbon isotope
120 chronology in Jämtland at Furuberget (see Section 2.3). From the existing CSCAN2019
121 collection, we selected 9 samples for quantitative wood anatomy analysis (QWA; *von Arx*
122 *et al.* [2016]) that spanned the full period from 1768 to 1798. The majority of the samples
123 chosen were mature (> 50 years old) at the time of the Laki eruption, while three were ju-
124 venile (< 33 years old). The crossdated chronology, ring-width measurements, and MXD
125 series were previously developed following standard dendrochronological procedures [*Linderholm and Gunnarson*, 2019]. The original MXD data were measured using an Itrax
126 Multiscanner (Cox Analytical Systems) with the opening width of the sensor slit set to
127 $20\ \mu\text{m}$ at each step [*Linderholm and Gunnarson*, 2019]. We used the original raw TRW
128 measurements to verify the dating of the 9 samples used here prior to processing the cores
129 for QWA analysis. For this study, we also created a Jämtland TRW chronology by fitting
130 a cubic smoothing spline with 50% frequency response cutoff at 30 years to a selection
131 of raw ring width measurements using the R-package *dplR* [*Bunn*, 2008; *R Core Team*,
132 2019].
133

134 We cut the wood samples to a thickness of $10\ \mu\text{m}$ using a rotary microtome (Microm
135 HM355S). The wood microsections were stained with a safranin solution, permanently
136 fixed in Eukitt, and prepared following standard procedures [*Gärtner and Schweingruber*,
137 2013; *von Arx et al.*, 2016]. Digital images of the microsections were produced at the

138 Swiss Federal Research Institute WSL in Birmensdorf, Switzerland, using a Zeiss Axio
139 Scan Z1. We measured the cell lumen area, cell wall thickness, and cell wall area for
140 the period 1768 to 1798 on all samples using the ROXAS (v3.1) image analysis software
141 [von Arx and Carrer, 2014; Prendin et al., 2017]. We excluded measurements of samples
142 with cell walls damaged during sampling or preparation. A total of 452,056 tracheid cells
143 were measured for the 30-year period. To create radial profiles of cell measurements for
144 analysis, we used a locally weighted smoothing (LOWESS) regression with a 10% span to
145 fit curves to the anatomical measurements [Cleveland, 1979]. Confidence intervals around
146 each curve were estimated from the residuals of the lowess fit. Although the eruption
147 and its environmental consequences did continue into 1784 [D'Arrigo et al., 2011; Zambri
148 et al., 2019b], for this study we consider 1783 the 'Laki year' and we use the remaining
149 30 years of wood anatomical data as a 'control' to provide context for growth anomalies
150 in 1783.

151 We calculated anatomical MXD (aMXD) as the maximum ratio between the cell wall
152 area and the full tracheid area (the sum of the cell wall area and cell lumen area) for
153 any given year at a range of measurement resolutions. We used the same series of 10 –
154 160 μm resolutions used by Björklund et al. [2019] to simulate those of other common
155 density measurement techniques. To calculate the 10 μm resolution values of a single year
156 for example, the raw cellular measurements are assigned 10 μm wide bands parallel to
157 the ring borders [Björklund et al., 2020]. Then, the median value of all cells within each
158 respective band is used as the representative value for that band. If the last band is less
159 than 10 μm then it is defined as the 10 μm adjacent to the terminal ring border [Björklund
160 et al., 2020]. For aMXD as with traditional MXD, a single value is therefore calculated for

161 each ring. The average aMXD of the 9 cores were used to create an ensemble of multiple
162 resolution aMXD chronologies. A number of studies have now shown that detrending
163 may not be necessary for some anatomical data [*Liang et al.*, 2013; *Carrer et al.*, 2018;
164 *Björklund et al.*, 2020]. We calculated the Pearson correlation coefficient between the
165 original CSCAN2019 MXD chronology and each aMXD chronology from 1768–1798. We
166 also applied a Mann-Kendall test ($\alpha = 0.05$) to the TRW, MXD, and aMXD chronologies
167 to identify any significant trends.

168 Intra-annual wood density fluctuations (IADFs) in the annual rings were identified both
169 visually and using an automatic statistical detection approach. For visual identification,
170 we used the classifications described in *Campelo et al.* [2007] and specifically looked for
171 earlywood-like cells in the middle of the latewood (IADF L) and earlywood-like cells at
172 the very end of the latewood (IADF L+). The same microsection images used to produce
173 the quantitative wood anatomy data were used for visual IADF identification (Figure 3).
174 For automatic detection of IADFs, we leveraged the increase in lumen area in latewood
175 that is caused by IADFs. We first created tracheidograms [*Vaganov*, 1990], standardized
176 to 100 cells, of lumen area for each core from 1768–1798. Then, we applied a 10-cell
177 Gaussian smoothing filter to the standardized tracheidograms. Years with an IADF were
178 then defined by a peak in the smoothed lumen area tracheidogram in the last 20% of the
179 ring.

2.2. Climate data

180 In order to evaluate the climate signal contained in wood anatomy and wood density
181 series from the 18th century, as well as the potential for short-term weather fluctua-
182 tions to affect wood anatomy [e.g. *Piermattei et al.*, 2020], we retrieved historical average

183 monthly adjusted temperature data for the Uppsala (59.88°N , 17.62°E, 27 m a.s.l.),
184 Trondheim/Vaernes (63.50°N , 10.90°E, 12 m a.s.l.), and Trondheim/Tyholt (63.41°N
185 , 10.45°E, 122 m a.s.l.) climate stations from the Berkeley Earth compilation [BEST;
186 *Lawrimore et al.*, 2011; *Menne et al.*, 2018; *Rohde and Hausfather*, 2020]. The Uppsala
187 station is nearly 500 km away from the Jämtland sampling site and the Trondheim sta-
188 tions are located on the west side of the Scandinavian mountains, where climate differs
189 from Jämtland. To estimate the relationship between climate at the Jämtland sampling
190 site and Uppsala and Trondheim, we also retrieved modern average monthly tempera-
191 ture data for the nearby Östersund (63.16°N , 14.40°E, 367 m a.s.l.) and Höglekardalen
192 (63.08°N , 13.75°E, 592 m a.s.l.) climate stations from the Berkeley Earth compilation
193 [BEST; *Lawrimore et al.*, 2011; *Menne et al.*, 2018; *Rohde and Hausfather*, 2020]. We av-
194 eraged the data from the Trondheim/Vaernes and the Trondheim/Tyholt stations due to
195 their proximity (25 km distance) and similarity ($r = 0.99$ for the 1768–1798 period), and
196 to compensate for missing values in each record. We calculated the Pearson correlation
197 coefficient between the monthly data at both climate stations and the multiple resolution
198 aMXD and CSCAN2019 MXD chronologies from 1768–1798. We also retrieved histor-
199 ical homogenized and adjusted daily mean temperature data for Stockholm (59.35°N ,
200 18.05°E) from the Bolin Centre Database [*Moberg, Anders*, 2020]. Summer temperatures
201 in that series have been adjusted to account for a previously identified warm bias in the
202 observations [*Moberg et al.*, 2003].

2.3. Carbon isotope data

203 Here we use the existing $\delta^{13}\text{C}$ record of Scots pine from the Furuberget site in the central
204 Scandinavian Mountains (63.17°N , 13.50°E – Figure 2) as an additional environmental

205 proxy to compare against the MXD chronologies [Seftigen *et al.*, 2011]. This $\delta^{13}\text{C}$ series
 206 was previously found to have a strong positive correlation with summer temperatures from
 207 1901 to 2000 across Jämtland and eastern Norway [Seftigen *et al.*, 2011]. We subtracted
 208 3‰ from the $\delta^{13}\text{C}$ series to account for the conversion of leaf carbohydrate to wood, and
 209 then converted this leaf-corrected $\delta^{13}\text{C}$ to isotopic discrimination ($\Delta^{13}\text{C}$) using Equation
 210 1 [Leavitt and Long, 1982; Mathias and Thomas, 2018; Belmecheri and Lavergne, 2020].

$$\Delta^{13}\text{C} = \left(\frac{\delta^{13}\text{C}_{air} - \delta^{13}\text{C}_{plant}}{1 + \frac{\delta^{13}\text{C}_{plant}}{1,000}} \right) \quad (1)$$

211 For $\delta^{13}\text{C}_{air}$ we used $\delta^{13}\text{C}O_2$ compiled by Belmecheri and Lavergne [2020], who interpo-
 212 lated pre-1850 $\delta^{13}\text{C}O_2$ annual values using the Bauska *et al.* [2015] and Eggleston *et al.*
 213 [2016] reconstructions. We calculated the Pearson correlation coefficient between $\Delta^{13}\text{C}$
 214 and the multiple resolution aMXD and CSCAN2019 MXD chronologies from 1768–1798,
 215 both including and excluding the post-eruption years 1783, 1784, and 1785.

2.4. X-ray fluorescence

216 We conducted X-ray fluorescence (XRF) analysis on three tree-ring core samples in
 217 order to test for the presence of a potential dendrochemical response from the impact of
 218 the acidic haze. Two trees were young (< 33 years old) and one tree was mature (> 100
 219 years old) at the time of the eruption. These three cores were also used for QWA analysis.
 220 Tree rings can be promising targets for detecting sulfur pollution and may be used to
 221 identify volcanic events [Pearson *et al.*, 2005, 2009; Fairchild *et al.*, 2009; Hevia *et al.*,
 222 2018; Binda *et al.*, 2021]. Because sulfur is structurally fixed in the wood, it can be a
 223 reliable indicator of environmental pollution [Fairchild *et al.*, 2009]. However, the final

224 amount of sulfur in the woody tissue is affected by the different sources and pathways to
225 the tree. Pine needles take up sulfur directly from the atmosphere whereas nutrients for
226 wood growth come from soil water, which are additionally subject to site conditions like
227 soil alkalinity [Fairchild *et al.*, 2009; Hevia *et al.*, 2018]. XRF is non-destructive while
228 providing detection of multiple different elements and has an adjustable spatial resolution
229 [Smith *et al.*, 2008]. We carried out XRF analysis using IXRF System’s Atlas Micro-
230 XRF unit, making a series of area scans of approximately 3 mm wide by 10 mm long
231 with a point dwell of 800 micro-seconds at 20 micron resolution. The primary excitation
232 source was 50 kV/50 W/1 mA with a Rh target. The instrument uses X-rays to excite
233 the surface of the sample, which produces characteristic X-rays that are at measurable
234 energies specific to the elements present. By moving the sample under the X-ray source at
235 regular intervals, a map of relative elemental abundances on the core surface is produced
236 [Pearson *et al.*, 2020].

3. Results

3.1. Quantitative Wood Anatomy

237 The original complete TRW chronology ($N = 24$ cores; Linderholm and Gunnarson
238 [2019]) and the average raw TRW of our QWA subset ($N = 9$ cores) are significantly and
239 positively correlated over their common interval (1768–1798, $r = 0.65$, $p < 0.01$; Figure
240 4a). Both show a sharp decrease in ring width after 1783. Based on our Mann-Kendall
241 test, the raw TRW series of our QWA subset has a significant downward trend over the pe-
242 riod 1768 to 1798 CE, which is likely in part an age-related growth effect, while none of the
243 aMXD chronologies have a significant trend. The high resolution aMXD chronologies from
244 this study are significantly positively correlated ($p < 0.01$) and are very similar to the orig-

245 inal MXD chronology [*Linderholm and Gunnarson, 2019*], except in 1783 and 1784. The
246 very high-resolution aMXD chronologies (aMXD10 – aMXD40) have a 1783 value that is
247 actually lower than 1784, while at lower measurement resolutions (aMXD50 – aMXD160),
248 1783 has a higher aMXD value than 1784 (Figure 4b,c) and is in better agreement with
249 the existing traditional MXD time series [*Linderholm and Gunnarson, 2019*]. Irrespective
250 of resolution, all of the aMXD chronologies are significantly and positively correlated with
251 the CSCAN2019 MXD chronology; the correlation coefficient increases from the higher-
252 resolution aMXD (aMXD20m, $r = 0.74$) to lower-resolution aMXD (aMXD160, $r = 0.92$;
253 Figure 5).

254 Examination of the wood anatomy in 1783 reveals the cause of these differences: an
255 IADF in the later half of the ring, associated with a band of latewood cells with larger
256 than average lumina that is followed by anomalously thin cell walls during the last part
257 of growth (Figure 3). For the late 18th century, the automated IADF detection method
258 identifies a slightly greater number of total IADFs overall compared to the simple visual
259 identification method (Figure 6). Using either method, however, 1783 has the highest
260 occurrence of IADFs in the 1768–1798 period. With automatic detection, 1783 has IADFs
261 in 5 out of 9 cores. With visual identification, 1783 has IADFs in 6 out of 9 cores. For
262 non-Laki years, the largest number of cores with an IADF detected were 2 (visual) or
263 3 (automated). One sample (Fb06_20d) had very narrow rings and therefore no IADFs
264 could be observed with the visual detection method.

265 Intra-annual profiles of lumen area and cell wall area – the individual components
266 that make up the anatomical density – reveal the cellular-level drivers of the IADFs in
267 1783 (Figure 7). While the 1783 Laki lumen area is actually larger than in non-eruption

268 control years for the first 50% of the total ring width, at between 60% to 80% of the total
269 ring width the lumen area drops suddenly below the control (Figure 7a), indicating a
270 premature end to the enlarging phase of xylogenesis for these cells. This rapid reduction is
271 accompanied by a simultaneous decline in the cell wall area (Figure 7b), further indicating
272 that cambial activity became suddenly disrupted at this time. While the Laki year lumen
273 area plateaued and rose slightly above the control year median for the last 15% of the
274 total ring width, the Laki cell wall area does not make a similar recovery and remains
275 below the non-eruption year median. The briefly higher density wood in the Laki year
276 at 65%–80% of the total ring width (Figure 7c) is therefore associated with the abrupt
277 decline in lumen area that defines the start of the IADF. For the remainder of the growing
278 season, the declining cell wall area combined with the plateau in lumen area resulted in
279 the low density measured in the last 15% of the 1783 ring.

3.2. Climate data

280 For the 1768–1798 period during the latter half of the Little Ice Age, the Stockholm,
281 Uppsala, and Trondheim stations experienced cool summers with temperatures rising
282 above 0 °C by April (Figure 8). Temperatures for 1783 were higher than the 1768–1798
283 average, with notably higher temperatures particularly in April, July, and September at
284 the Trondheim stations (Figure 8b). Temperatures in 1784 were consistently lower than
285 the 1768–1798 average particularly in the winter of that year at both stations (Figure
286 8a,b). Daily data also show that Stockholm temperatures in the summer of 1783 were
287 generally higher than the 1768–1798 average, except for a brief period in the beginning
288 of August when temperature was on average 2.48 °C below normal over a period of 5
289 days (Figure 8c). A comparison of modern weather observations from Östersund and

290 Högkardalen suggests the Jämtland tree-ring site is 0–2.5°C cooler than Trondheim and
291 3–5°C cooler than Uppsala.

292 All of the aMXD chronologies and CSCAN2019 are significantly and positively corre-
293 lated with August temperature at both historical stations over the full 1768–1798 period
294 (Figure 9). The highest correlation ($r = 0.65$) is between CSCAN2019 and August tem-
295 perature at Uppsala, and the strongest aMXD correlation ($r = 0.60$) is between aMXD80
296 and August temperature at Uppsala. Both CSCAN2019 and the lower resolution aMXD
297 (aMXD80–aMXD160) series have a broader seasonal range of months with significant
298 correlations at the Uppsala station, although interestingly not at Trondheim (Figure 9a).
299 The correlations with historical climate data from the 18th century are stronger overall
300 if 1783 is excluded (not shown).

3.3. Carbon isotope data

301 The $\Delta^{13}\text{C}$ series has a large negative excursion at 1783–1785, with the largest decrease
302 in isotopic discrimination in 1784 (Figure 10). If we consider the entirety of the 1768–
303 1798 period, there is no significant correlation between any of the MXD chronologies
304 and the $\Delta^{13}\text{C}$ series (Table 1). However, when we simply exclude 1783, 1784, and 1785
305 from the calculation, the expected [*Gagen et al.*, 2007; *Seftigen et al.*, 2011] significant
306 negative correlation between the MXD chronologies and $\Delta^{13}\text{C}$ emerges. The absolute
307 value of the correlation coefficient generally increases from high-resolution aMXD to low-
308 resolution aMXD (Table 1), with the weakest negative correlation at aMXD20 ($r = -0.35$,
309 $p = 0.07$), and the strongest negative correlation at aMXD160 ($r = -0.62$, $p < 0.01$). All
310 correlations with 1783, 1784, and 1785 excluded are significant at $p \leq 0.07$ (Table 1).

3.4. X-ray fluorescence

311 Both sulfur and chlorine were below detection limits for our XRF analysis of these
312 samples. Elements such as As, Br, Cu, and Zn – which could reflect an acidification
313 response – do show a slight decrease in the latewood of the 1783 and 1784 rings, but
314 this could also result from lower latewood density in these rings [*Pearson et al.*, 2009].
315 *Pearson et al.* [2006] was similarly not able to detect a clear influence of the 1875 eruption
316 of the Icelandic volcano Askja on trees growing downwind in central Sweden. Even for
317 forests subject to high levels of anthropogenically or volcanically produced pollutants,
318 dendrochemical analyses have shown mixed results [*Watmough*, 1997; *Watt et al.*, 2007;
319 *Rocha et al.*, 2020], with a number of complex environmental processes in play. Even
320 when eruptions do leave a geochemical trace in annual rings, individual trees may record
321 different signals [*Sheppard et al.*, 2009]. Our dendrochemistry results, while compatible
322 with an acid deposition hypothesis, were inconclusive, and cannot be strongly argued to
323 support the direct impact of the acidic Laki haze on wood anatomical anomalies in 1783.

4. Discussion

4.1. Measurement resolution, extreme events, and the disruption of wood formation

324 Calculating aMXD using multiple different resolutions permits us to identify the com-
325 plicated and abnormal intra-annual tree-ring response to the Laki volcanic eruption (Fig-
326 ure 4), which in turn allows us to better understand the discrepancy between historical
327 observations and traditional MXD (Figure 1). The MXD from Jämtland used in the
328 *Luterbacher et al.* [2016] reconstruction and others [e.g. *Anchukaitis et al.*, 2017] were
329 measured using the Itrax wood scanner [*Gunnarson et al.*, 2011; *Linderholm and Gun-*

330 *narson*, 2019]. While the measurements were taken at nominal 20 μm steps [*Linderholm*
331 *and Gunnarson*, 2019], *Björklund et al.* [2019] calculated an effective or apparent resolu-
332 tion for Itrax between 100 and 120 μm . The 10 μm resolution aMXD typically calculates
333 the density in very last section of the latewood, which is relatively low in 1783 CE, as seen
334 in Figure 3. The low MXD measured by the Itrax or the low resolution aMXD in 1783 is
335 caused by the inclusion of this low density section in the very last portion of the latewood
336 but then is ameliorated in part by incorporating the higher density portion of the IADF
337 (Figure 4). In other words, the lower effective resolution of the Itrax data coincidentally
338 compensates somewhat for the very low wood density detected by our highest resolution
339 aMXD calculations because the Itrax also incorporates the higher density portion of the
340 IADF. Our use of the high resolution aMXD measurements shows that IADFs in 1783
341 are caused by disruptions to the normal anatomical structure of the annual ring. When
342 the normal wood formation is disturbed, as it is here after the eruption, the expected
343 relationship between summer temperature and traditional MXD measurements appears
344 to be altered.

4.2. Potential causes of low MXD and IADFs in 1783

345 IADFs are the result of deviations from the normal growing season patterns of xylogen-
346 esis [*Mayer et al.*, 2020; *De Micco et al.*, 2016]. The characteristic density fluctuations of
347 IADFs can form due to changes in cell differentiation or bimodal cambial activity: in our
348 case, cambial activity declines and smaller abnormal cells are produced due to detrimental
349 growing conditions [*Wimmer et al.*, 2000; *Battipaglia et al.*, 2016; *De Micco et al.*, 2016;
350 *Morino et al.*, 2021]. Anatomical anomalies like IADFs are generally formed when trees
351 experience stressful conditions, including drought, defoliation, or frost events [*Cuny et al.*,

2014; *Fritts*, 1976]. IADFs have been commonly linked to changes in moisture availabil-
ity in trees from Mediterranean or bimodal precipitation monsoon regions [*Morino et al.*,
2021], but are rarely found in boreal forest trees [*Battipaglia et al.*, 2016]. In boreal forests
however, the occurrence of IADFs can be the result of defoliation from pollution or sud-
den cold events [*Kurczyńska et al.*, 1997; *Kozlov and Kisternaya*, 2004]. IADFs have been
more commonly observed in wide rings [*Battipaglia et al.*, 2016; *De Micco et al.*, 2016].
The IADFs we observe in 1783 originate from an initial sharp decline in lumen area in
the later section of the ring, concomitant with a decline in cell wall area in the latewood,
which results in a temporary increase in anatomical density followed by a reduction at
the very end of the year, relative to the control years (Figure 7).

Based on multiple lines of evidence discussed in detail below, we hypothesize that the
high prevalence of IADFs in 1783 was most likely caused by acid damage from the volcanic
eruption and is linked to the anomalous MXD values in that year. Our assessment rules
out temperature changes through comparison between the multiple MXD chronologies,
historical observations, and the $\Delta^{13}\text{C}$ record. We cannot however conclusively parse the
possible effect of changes to light availability as the Furuberget $\Delta^{13}\text{C}$ chronology appears
to be overwhelmed by the direct effect of the acidic haze.

We interpret the low MXD and high frequency of IADFs in 1783 to most likely be a
consequence of the direct and detrimental effect of the Laki eruption's acidic haze on tree
growth, as hypothesized by *Briffa et al.* [1988]. Historical observations in Sweden and
Norway at that time noted acidic haze and concurrent vegetation damage [*Thorarinsson*,
1981; *Grattan and Pyatt*, 1994; *Laufeld*, 1994; *Demarée and Ogilvie*, 2001]. In Trond-
heim, tree leaves were described as “burnt” and vegetation “withered” after acid rain

375 and fog deposition respectively [*Demarée and Ogilvie, 2001*]. In Sweden, the dry fog was
376 observed to be “injurious to the vegetation” and that it “damaged the trees” and caused
377 plants to “wither and drop their leaves” [*Thorarinsson, 1981*]. Volcanic pollutants in-
378 cluding SO₂ and H₂S are known to damage conifer needles, which leads to a reduction
379 of stomatal aperture and potentially defoliation and tree death [*Bartirromo et al., 2012*].
380 SO₂ and SO₄-induced damage to needle stomata also limits photosynthetic CO₂ fixation
381 and causes preferential uptake of ¹³C [*Martin et al., 1988; Thomas et al., 2013; D’Arcy*
382 *et al., 2019*], which is consistent with the decrease in carbon isotope discrimination we
383 observe in the Furuberget $\Delta^{13}\text{C}$. Trees under consistent industrial sulfur pollution have
384 also displayed reduced MXD and increased occurrences of IADFs compared to trees at
385 non-polluted sites [*Kurczyńska et al., 1997; Wimmer, 2002*]. A study by *Myśkow et al.*
386 [2019] demonstrated that pollutant fog deposition resulted in decreased cambial activ-
387 ity, leading to the formation of narrower annual rings as we observe at Jämtland in the
388 years following the eruption (Figure 4). Ring-width suppression and needle damage in
389 *P. sylvestris* has similarly been reported in association with artificial smoke, containing
390 chlorosulfonic acid, used to conceal the location of the German battleships *Tirpitz* during
391 the Second World War [*Hartl et al., 2019*] and as the result of insect induced defoliation
392 [*Axelson et al., 2014; Watanabe and Ohno, 2020*]. A number of investigators have found
393 additionally that latewood width, latewood density, and cell wall thickness can all be
394 reduced by defoliation [*Esper et al., 2007; Arbellay et al., 2018; Castagneri et al., 2020*].

395 A combination of the atmospheric conditions at the time of the Laki eruption and also
396 potentially the influence of site topography likely led to long-lasting and effective volcanic
397 pollutant deposition at our study site. Volcanic gas concentration and persistence have

398 a direct effect on the severity of damage to vegetation [*Delmelle, 2003; Bartiromo et al.,*
399 2012]. Acidified fog can potentially have 10 times the solute concentration compared to
400 rain, and has greater capacity for vegetation damage [*Delmelle, 2003*]. The high pres-
401 sure cell and atmospheric blocking over Europe at the time of the Laki eruption also
402 led to a more persistent sulfuric surface haze [*Thordarson and Self, 2003; Zambri et al.,*
403 2019a]. Modeling experiments show high surface sulfate aerosol concentrations over cen-
404 tral Sweden throughout the summer [*Chenet et al., 2005*] and historical observations from
405 Stockholm first note a “dry fog” on June 24, which then continued every day for a month,
406 except for four days at the end of June/early July [*Thorarinsson, 1981; Thordarson and*
407 *Self, 2003*]. Model simulations of the Laki eruption show peak sulphate loading in the
408 upper troposphere/lower stratosphere in August [*Oman et al., 2006; Zambri et al., 2019b*],
409 the time period when temperature would otherwise normally be the primary influence on
410 MXD (Figure 9). Previous studies have also found a positive relationship between ele-
411 vation and sulfate deposition, with fogwater deposition more significant than deposition
412 from precipitation at higher elevations [*Walmsley et al., 1970; Lükewille and Semb, 1997*].
413 While the trees in the full dataset were collectively sampled over a wide area, the majority
414 of the trees used here for QWA analysis were sampled on the top of a small peak at ~650
415 m a.s.l. [*Linderholm and Gunnarson, 2019*], possibly making them even more susceptible
416 to the direct effects of the haze [*Delmelle, 2003*].

417 In theory, a sudden or transient cold period could also cause low density in the very last
418 section of the 1783 ring [c.f. *Piermattei et al., 2020; Edwards et al., 2021*]. At lower mea-
419 surement resolution both traditional MXD and aMXD chronologies reflect temperatures
420 integrated over the entire summer, while the high resolution aMXD chronologies capture

421 the anatomical characteristics of only late growing season August temperature (Figure 9).
422 The higher resolution aMXD chronologies (Figure 4b) are therefore capable of capturing a
423 monthly or even sub-monthly climate signal caused by a brief cold period at the end of the
424 growing season, as occurred in Alaska following the Laki eruption [*Edwards et al.*, 2021].
425 The monthly data from the Uppsala and Trondheim stations may be too coarse however
426 to properly identify such a period. Daily data from Stockholm does show a 5-day period
427 of negative temperature anomalies (-2.48°C below climatology over the 5-day period) in
428 the beginning of August (Figure 8c). However, this period is unlikely to be long enough
429 nor sufficiently severe to cause the anomalous wood anatomy and low MXD seen in the
430 1783 ring [*Begum et al.*, 2012]. Low August and September temperatures that cause an
431 early end to the growing season, as well as ephemeral cold snaps, have been previously
432 linked to lower MXD and associated with 'light rings' [*Szeicz*, 1996; *Gindl et al.*, 2000;
433 *Vaganov et al.*, 2006; *Edwards et al.*, 2021] or 'blue rings' [*Piermattei et al.*, 2015; *Matison*
434 *et al.*, 2020; *Piermattei et al.*, 2020; *Björklund et al.*, 2021], neither of which are observed
435 in the 1783 rings. Damage to vegetation from Laki acid deposition was often at the time
436 erroneously attributed to overnight frost across Europe, including in Sweden [*Thordarson*
437 *and Self*, 2003]. But because early morning and evening temperatures were recorded to
438 be well above freezing ($10^{\circ}\text{C} - 15^{\circ}\text{C}$), it is unlikely that temperatures would drop below
439 freezing in the few hours between measurements [*Thordarson and Self*, 2003]. There is
440 a negative temperature anomaly at the beginning of May in Stockholm (Figure 8c) and
441 mild frosts in late spring/early summer have been previously linked to IADF occurrence
442 [*Kozlov and Kisternaya*, 2004]. However, early season climate conditions are more com-
443 monly associated with IADFs defined by latewood-like cells within the earlywood, rather

444 than the type of IADFs we see in 1783, which is defined by earlywood-like cells within
445 the latewood [*Campelo et al.*, 2007; *De Micco et al.*, 2016].

446 An alternative hypothesis is that the low MXD in 1783 could be caused by a decrease in
447 light availability after the Laki eruption, overwhelming the proxy's normal temperature
448 response. For instance, *Tingley et al.* [2014] suggest that low MXD in years following
449 volcanic eruptions could be caused by the additional effect from the reduction in light. In
450 contrast, the Furuberget $\Delta^{13}\text{C}$ record (Figure 10) would conventionally be interpreted as
451 indicating an *increase* in light availability during and after the Laki eruption (Figure 10),
452 as tree-ring $\delta^{13}\text{C}$ records from this region have been shown to positively covary with sun-
453 shine metrics [*Gagen et al.*, 2007; *Seftigen et al.*, 2011; *Loader et al.*, 2013]. The negative
454 $\Delta^{13}\text{C}$ excursion may be because an increase in diffuse radiation caused by light scattering
455 from volcanic aerosols [*Robock*, 2005] actually increased photosynthetic capacity. Diffuse
456 radiation has been hypothesized to lead to more efficient photosynthesis [*Gu et al.*, 2003;
457 *Mercado et al.*, 2009] and would presumably result in an increase in MXD [*Robock*, 2005].
458 There are however contrasting findings in this regard (e.g. *Knohl and Baldocchi* [2008])
459 and furthermore, there is no evidence from either TRW or MXD that growth conditions
460 during the summer of 1783 were more favorable due to increased diffuse light. The neg-
461 ative $\Delta^{13}\text{C}$ excursion observed in 1783 is the expected response to a decrease in carbon
462 isotope discrimination caused by accounts of historical acid deposition [*Rayback et al.*,
463 2020]. Other tree-ring $\delta^{13}\text{C}$ records from further north in Fennoscandia however are un-
464 remarkable in 1783 and do not indicate any consistent changes in cloud cover or light
465 availability over the broader region [*Young et al.*, 2012; *Loader et al.*, 2013]. Thus, while
466 we cannot eliminate a potential role for changing light availability during the eruption in

467 1783, the carbon isotope evidence from Furuberget is most consistent with the expected
468 response to direct damage to trees from acidic haze.

469 Lumen area is also normally correlated with day length over the course of the growing
470 season, with the longer photoperiod of summer promoting the production of auxin, the
471 phytohormone responsible for cell growth and extensibility [*Cuny et al.*, 2014; *Cuny and*
472 *Rathgeber*, 2016; *Rathgeber et al.*, 2016; *Buttò et al.*, 2021]. *Oman et al.* [2006] simulated a
473 strong decrease in surface shortwave radiation during the summer 1783 and contemporary
474 accounts report the ‘sky was overspread with a dark dry fog’ [*Brayshay and Grattan*, 1999].
475 However, it is not clear what the response of the cambium might be to a *sudden* change in
476 photosynthetically available radiation during the eruption or how this would be reflected
477 in the lumen anatomy for that year. Experimental and observational evidence of the
478 cambial response to sudden changes in light following volcanic eruption may help further
479 parse the relative contributions to the haze itself and the concomitant alteration of surface
480 radiation.

4.3. Abnormal wood anatomy disrupts MXD temperature signals

481 While one would expect to see high MXD values in 1783 given the high temperatures
482 recorded across Scandinavia (Figure 8), the direct effects of the volcanic haze appear to
483 be the best explanation for the disrupted climate signal. In the first 50% of the total
484 ring width, the 1783 lumen area is higher than the control period average, as might be
485 expected during a warm spring and the generally favorable growing conditions seen in
486 historical records, but it then sharply declines at 60% through the annual ring (Figure
487 7a). This decrease in lumen area leads to a temporary increase in density, but reduced
488 cell wall area ultimately leads to the low density in the last 15% of total ring width and

489 the low MXD value in 1783 (Figure 7). *Vejpustková et al.* [2017] found that lumen width,
490 cell wall thickness, and cell number all decreased following an industrial SO₂ pollution
491 event and *Mysłkow et al.* [2019] found that earlywood cell width and lumen area decreased
492 during intense pollutant deposition. Other studies have also shown that industrial sulfur
493 pollution leads to reduced MXD and increased occurrence of IADFs compared to trees at
494 non-polluted sites [*Evertsen et al.*, 1986; *Kurczyńska et al.*, 1997; *Wimmer*, 2002]. In 1783
495 the cell wall area in the Jämtland trees decreases below the non-eruption year average
496 at the same time as the lumen area declines but never recovers, which ultimately leads
497 to the low MXD for the year (Figure 7b). Normally, we expect cell wall area to remain
498 approximately fixed throughout the ring except for the very last cells that respond to
499 climate conditions [*Cuny et al.*, 2014], so the decrease in cell wall area and the other
500 anatomical anomalies that we observe in 1783 indicates a disturbance of the normal wood
501 formation process.

5. Conclusion

502 By using wood anatomical data in combination with stable carbon isotope data and
503 historical observations, we identified the cause of the discrepancy between historical ob-
504 servations and traditional MXD chronologies following the 1783 Laki eruption. We found
505 both a high prevalence of IADFs and reduced lumen and cell wall area in the latewood
506 of 1783, which we interpret to most likely be the consequence of the damaging effects
507 of volcanic acid deposition on wood formation processes. In contrast, 1784 shows the
508 expected response to cooling that year – lower MXD – and better agrees with historical
509 records. The decline in tree-ring width in 1784 and for several years afterward might also

510 reflect the ongoing effects of the acid induced defoliation that occurred in 1783 [*Axelsson*
511 *et al.*, 2014; *Hartl et al.*, 2019].

512 The results of this study have implications for the interpretation of tree-ring records
513 following proximal volcanic eruptions. In the case of tree rings formed during the Laki
514 eruption, we clearly demonstrate that the normal climate/MXD relationship is disrupted
515 or obfuscated by the anatomical consequences of what is most likely the direct regional
516 effects of acidic haze. Under normal circumstance, the high resolution density estimates
517 made possible by quantitative wood anatomy can provide very precise estimates of past
518 temperature variability and trends [*Björklund et al.*, 2020], but the ability to vary the
519 effective resolution of these measurements also suggests a potential approach for identify-
520 ing anomalous years associated with rare disturbances or extreme environmental events.
521 However, it is not yet clear that it is possible to recover the ‘true’ temperature signature
522 from rings where anatomical anomalies reflect a non-climate cause. Further work is nec-
523 essary to determine how best to use aMXD records to analyze and quantify these extreme
524 years, but our study already suggests that screening anatomical series for anomalies can
525 lead to an evaluation of potentially confounding factors for climate reconstructions. In
526 the case of the Laki eruption specifically, wood anatomy allows us to understand why
527 existing tree-ring reconstructions of summer temperature using MXD do not agree with
528 historical records and observations. In addition to the previously established effects of
529 the Laki eruption haze on human health, our study underlines the potential detrimental
530 effect of acid volcanic haze on forest vegetation, underscoring the wide-ranging impact
531 that such eruptions can have across a large region.

Data Availability

532 The tree-ring data that support the findings of this study are available in the Interna-
533 tional Tree-Ring Data Bank (ITRDB) at the NOAA/World Data Service for Paleoclima-
534 tology archives.

535 **Acknowledgments.** KJA thanks Alan Robock and Brian Zambri for discussions at
536 the Past Global Changes (PAGES) ‘Volcanic Impacts on Climate and Society’ (VICS)
537 meeting in Cambridge about the reconstructed climate discrepancy in Europe during the
538 Laki eruption. We thank Talia Anderson for assisting with visual IADF identification and
539 Soumaya Belmecheri for additional discussions about carbon isotopes. JE and KJA were
540 partially supported by NSF P2C2 grant AGS-2102993. KS and GvA were supported by
541 the Swiss National Science Foundation SNSF (grant no. 200021_182398, XELLCLIM).

References

- 542 Anchukaitis, K. J., R. Wilson, K. R. Briffa, U. Buntgen, E. R. Cook, R. D’Arrigo, N. Davi,
543 J. Esper, D. Frank, B. E. Gunnarson, G. Hegerl, S. Helama, S. Klesse, P. J. Krusic,
544 H. W. Linderholm, V. Myglan, T. J. Osborn, P. Zhang, M. Rydval, L. Schneider,
545 A. Schurer, G. Wiles, and E. Zorita (2017), Last millennium Northern Hemisphere
546 summer temperatures from tree rings: Part II, spatially resolved reconstructions, *Qua-*
547 *ternary Science Reviews*, *163*, 1–22, doi:10.1016/j.quascirev.2017.02.020.
- 548 Arbella, E., I. Jarvis, R. D. Chavardès, L. D. Daniels, and M. Stoffel (2018), Tree-ring
549 proxies of larch bud moth defoliation: latewood width and blue intensity are more
550 precise than tree-ring width, *Tree physiology*, *38*(8), 1237–1245.

- 551 Auken, M. R., R. S. J. Sparks, L. Siebert, H. S. Crossweller, and J. Ewert (2013), A
552 statistical analysis of the global historical volcanic fatalities record, *Journal of Applied*
553 *Volcanology*, 2(1), doi:10.1186/2191-5040-2-2.
- 554 Axelson, J., A. Bast, R. Alfaro, D. Smith, and H. Gärtner (2014), Variation in wood
555 anatomical structure of Douglas-fir defoliated by the western spruce budworm: a case
556 study in the coastal-transitional zone of British Columbia, Canada, *Trees*, 28(6), 1837–
557 1846.
- 558 Bartiromo, A., G. Guignard, M. R. B. Lumaga, F. Barattolo, G. Chiodini, R. Avino,
559 G. Guerriero, and G. Barale (2012), Influence of volcanic gases on the epidermis of
560 *Pinus halepensis* Mill. in Campi Flegrei, Southern Italy: A possible tool for detecting
561 volcanism in present and past floras, *Journal of Volcanology and Geothermal Research*,
562 233-234, 1–17, doi:https://doi.org/10.1016/j.jvolgeores.2012.04.002.
- 563 Battipaglia, G., F. Campelo, J. Vieira, M. Grabner, V. De Micco, C. Nabais, P. Cherubini,
564 M. Carrer, A. Bräuning, K. Čufar, et al. (2016), Structure and function of intra-annual
565 density fluctuations: mind the gaps, *Frontiers in plant science*, 7, 595.
- 566 Bauska, T. K., F. Joos, A. C. Mix, R. Roth, J. Ahn, and E. J. Brook (2015), Links
567 between atmospheric carbon dioxide, the land carbon reservoir and climate over the
568 past millennium, *Nature Geoscience*, 8(5), 383–387.
- 569 Begum, S., S. Nakaba, M. A. Islam, Y. Yamagishi, R. Funada, et al. (2012), Effects of
570 low temperature in reactivated cambial cells induced by localized heating during winter
571 dormancy in conifers., *American Journal of Plant Physiology*, 7(1), 30–40.
- 572 Belmecheri, S., and A. Lavergne (2020), Compiled records of atmospheric CO₂ concentra-
573 tions and stable carbon isotopes to reconstruct climate and derive plant ecophysiological

- 574 indices from tree rings, *Dendrochronologia*, 63, 125,748.
- 575 Binda, G., A. Di Iorio, and D. Monticelli (2021), The what, how, why, and when of
576 dendrochemistry:(paleo) environmental information from the chemical analysis of tree
577 rings, *Science of The Total Environment*, 758, 143,672.
- 578 Björklund, J., M. V. Fonti, P. Fonti, J. Van den Bulcke, and G. von Arx (2021), Cell wall
579 dimensions reign supreme: cell wall composition is irrelevant for the temperature signal
580 of latewood density/blue intensity in Scots pine, *Dendrochronologia*, 65, 125,785.
- 581 Björklund, J., G. Arx, D. Nievergelt, R. Wilson, J. V. den Bulcke, B. Günther,
582 N. J. Loader, M. Rydval, P. Fonti, T. Scharnweber, L. Andreu-Hayles, U. Büntgen,
583 R. D'Arrigo, N. Davi, T. D. Mil, J. Esper, H. Gärtner, J. Geary, B. E. Gunnarson,
584 C. Hartl, A. Hevia, H. Song, K. Janecka, R. J. Kaczka, A. V. Kirilyanov, M. Kochbeck,
585 Y. Liu, M. Meko, I. Mundo, K. Nicolussi, R. Oelkers, T. Pichler, R. Sánchez-Salguero,
586 L. Schneider, F. Schweingruber, M. Timonen, V. Trouet, J. V. Acker, A. Verstege,
587 R. Villalba, M. Wilmking, and D. Frank (2019), Scientific merits and analytical
588 challenges of tree-ring densitometry, *Reviews of Geophysics*, 57(4), 1224–1264, doi:
589 10.1029/2019rg000642.
- 590 Björklund, J., K. Seftigen, P. Fonti, D. Nievergelt, and G. von Arx (2020), Dendroclimatic
591 potential of dendroanatomy in temperature-sensitive *Pinus sylvestris*, *Dendrochronolo-*
592 *gia*, 60, 125,673, doi:10.1016/j.dendro.2020.125673.
- 593 Brayshay, M., and J. Grattan (1999), Environmental and social responses in Europe to the
594 1783 eruption of the Laki fissure volcano in Iceland: a consideration of contemporary
595 documentary evidence, *Geological Society, London, Special Publications*, 161(1), 173–
596 187, doi:10.1144/gsl.sp.1999.161.01.12.

- 597 Briffa, K. R., P. D. Jones, J. R. Pilcher, and M. K. Hughes (1988), Reconstructing summer
598 temperatures in northern Fennoscandia back to A.D. 1700 using tree-ring data from
599 Scots pine, *Arctic and Alpine Research*, *20*(4), 385–394.
- 600 Brown, S. K., M. Auker, and R. Sparks (2015), Populations around Holocene volcanoes
601 and development of a Population Exposure Index, in *Global Volcanic Hazards and Risk*,
602 pp. 223–232, Cambridge University Press Cambridge.
- 603 Budd, L., S. Griggs, D. Howarth, and S. Ison (2011), A fiasco of volcanic proportions?
604 Eyjafjallajökull and the closure of European airspace, *Mobilities*, *6*(1), 31–40.
- 605 Bunn, A. G. (2008), A dendrochronology program library in R (dplR), *Dendrochronologia*,
606 *26*(2), 115–124, doi:10.1016/j.dendro.2008.01.002.
- 607 Buttò, V., P. Rozenberg, A. Deslauriers, S. Rossi, and H. Morin (2021), Environmental
608 and developmental factors driving xylem anatomy and micro-density in black spruce,
609 *New Phytologist*, *230*(3), 957–971.
- 610 Campelo, F., C. Nabais, H. Freitas, and E. Gutiérrez (2007), Climatic significance of tree-
611 ring width and intra-annual density fluctuations in *Pinus pinea* from a dry Mediter-
612 ranean area in Portugal, *Annals of Forest Science*, *64*(2), 229–238.
- 613 Carlsen, H. K., A. Hauksdottir, U. A. Valdimarsdottir, T. Gíslason, G. Einarsdottir,
614 H. Runolfsson, H. Briem, R. G. Finnbjornsdottir, S. Gudmundsson, T. B. Kolbeinsson,
615 et al. (2012), Health effects following the Eyjafjallajökull volcanic eruption: a cohort
616 study, *BMJ open*, *2*(6).
- 617 Carlsen, H. K., E. Ilyinskaya, P. J. Baxter, A. Schmidt, T. Thorsteinsson, M. A. Pfeffer,
618 S. Barsotti, F. Dominici, R. G. Finnbjornsdottir, T. Jóhannsson, et al. (2021), Increased
619 respiratory morbidity associated with exposure to a mature volcanic plume from a large

- 620 Icelandic fissure eruption, *Nature Communications*, *12*(1), 1–12.
- 621 Carrer, M., L. Unterholzner, and D. Castagneri (2018), Wood anatomical traits high-
622 light complex temperature influence on *Pinus cembra* at high elevation in the East-
623 ern Alps, *International Journal of Biometeorology*, *62*(9), 1745–1753, doi:10.1007/
624 s00484-018-1577-4.
- 625 Castagneri, D., A. L. Prendin, R. L. Peters, M. Carrer, G. von Arx, and P. Fonti
626 (2020), Long-term impacts of defoliator outbreaks on larch xylem structure and tree-ring
627 biomass, *Frontiers in plant science*, *11*, 1078.
- 628 Chenet, A.-L., F. Fluteau, and V. Courtillot (2005), Modelling massive sulphate aerosol
629 pollution, following the large 1783 Laki basaltic eruption, *Earth and Planetary Science*
630 *Letters*, *236*(3-4), 721–731.
- 631 Cleveland, W. S. (1979), Robust locally weighted regression and smoothing scatterplots,
632 *Journal of the American Statistical Association*, *74*(368), 829–836.
- 633 Cuny, H. E., and C. B. Rathgeber (2016), Xylogenesis: coniferous trees of temperate
634 forests are listening to the climate tale during the growing season but only remember
635 the last words!, *Plant Physiology*, *171*(1), 306–317.
- 636 Cuny, H. E., C. B. K. Rathgeber, D. Frank, P. Fonti, and M. Fournier (2014), Kinetics
637 of tracheid development explain conifer tree-ring structure, *New Phytologist*, *203*(4),
638 1231–1241, doi:10.1111/nph.12871.
- 639 Damby, D. E., C. J. Horwell, G. Larsen, T. Thordarson, M. Tomatis, B. Fubini, and
640 K. Donaldson (2017), Assessment of the potential respiratory hazard of volcanic ash
641 from future icelandic eruptions: a study of archived basaltic to rhyolitic ash samples,
642 *Environmental Health*, *16*(1), 1–15.

- 643 D'Arrigo, R., R. Seager, J. E. Smerdon, A. N. LeGrande, and E. R. Cook (2011), The
644 anomalous winter of 1783-1784: Was the Laki eruption or an analog of the 2009-
645 2010 winter to blame?, *Geophysical Research Letters*, *38*(5), n/a–n/a, doi:10.1029/
646 2011gl046696.
- 647 D'Arrigo, R., R. Wilson, and K. J. Anchukaitis (2013), Volcanic cooling signal in tree
648 ring temperature records for the past millennium, *Journal of Geophysical Research:
649 Atmospheres*, *118*(16), 9000–9010, doi:10.1002/jgrd.50692.
- 650 Dawson, A. G., M. P. Kirkbride, and H. Cole (2021), Atmospheric effects in Scotland of
651 the AD 1783–84 Laki eruption in Iceland, *The Holocene*, *31*(5), 830–843.
- 652 De Micco, V., F. Campelo, M. De Luis, A. Bräuning, M. Grabner, G. Battipaglia, and
653 P. Cherubini (2016), Intra-annual density fluctuations in tree rings: how, when, where,
654 and why?, *IAWA Journal*, *37*(2), 232–259.
- 655 Delmelle, P. (2003), Environmental impacts of tropospheric volcanic gas plumes, *Geolog-
656 ical Society, London, Special Publications*, *213*(1), 381–399.
- 657 Demarée, G. R., and A. E. Ogilvie (2001), Bons Baisers d'Islande: Climatic, environmen-
658 tal, and human dimensions impacts of the Lakagígur eruption (1783–1784) in Iceland,
659 in *History and Climate*, pp. 219–246, Springer.
- 660 Durand, M., and J. Grattan (1999), Extensive respiratory health effects of volcanogenic
661 dry fog in 1783 inferred from European documentary sources, *Environmental Geochem-
662 istry and Health*, *21*(4), 371–376.
- 663 D'Arcy, F., É. Boucher, J. M. De Moor, J.-F. Hélie, R. Piggott, and J. Stix (2019),
664 Carbon and sulfur isotopes in tree rings as a proxy for volcanic degassing, *Geology*,
665 *47*(9), 825–828.

- 666 Edwards, J., K. J. Anchukaitis, B. Zambri, L. Andreu-Hayles, R. Oelkers, R. D'Arrigo, and
667 G. von Arx (2021), Intra-annual climate anomalies in Northwestern North America fol-
668 lowing the 1783–1784 CE Laki eruption, *Journal of Geophysical Research: Atmospheres*,
669 *126*(3), e2020JD033544, doi:<https://doi.org/10.1029/2020JD033544>, e2020JD033544
670 2020JD033544.
- 671 Eggleston, S., J. Schmitt, B. Bereiter, R. Schneider, and H. Fischer (2016), Evolution of
672 the stable carbon isotope composition of atmospheric CO₂ over the last glacial cycle,
673 *Paleoceanography*, *31*(3), 434–452.
- 674 Esper, J., U. Büntgen, D. C. Frank, D. Nievergelt, and A. Liebhold (2007), 1200 years
675 of regular outbreaks in alpine insects, *Proceedings of the Royal Society B: Biological*
676 *Sciences*, *274*(1610), 671–679.
- 677 Esper, J., L. Schneider, J. E. Smerdon, B. R. Schöne, and U. Büntgen (2015), Signals
678 and memory in tree-ring width and density data, *Dendrochronologia*, *35*, 62–70, doi:
679 10.1016/j.dendro.2015.07.001.
- 680 Esper, J., S. S. George, K. Anchukaitis, R. D'Arrigo, F. C. Ljungqvist, J. Luterbacher,
681 L. Schneider, M. Stoffel, R. Wilson, and U. Büntgen (2018), Large-scale, millennial-
682 length temperature reconstructions from tree-rings, *Dendrochronologia*, *50*, 81–90.
- 683 Evertsen, J., M. Mac Siurtain, and J. Gardiner (1986), The effect of industrial emission
684 on wood quality in norway spruce (*Picea abies*), *IAWA Journal*, *7*(4), 399–404.
- 685 Fairchild, I. J., N. J. Loader, P. M. Wynn, S. Frisia, P. A. Thomas, J. G. Laguard,
686 A. d. Momi, A. Hartland, A. Borsato, N. L. Porta, et al. (2009), Sulfur fixation in
687 wood mapped by synchrotron X-ray studies: implications for environmental archives,
688 *Environmental science & technology*, *43*(5), 1310–1315.

- 689 Frank, D., U. Büntgen, R. Böhm, M. Maugeri, and J. Esper (2007), Warmer early instru-
690 mental measurements versus colder reconstructed temperatures: shooting at a moving
691 target, *Quaternary Science Reviews*, *26*(25-28), 3298–3310.
- 692 Franklin, B. (1785), *Meteorological imaginations and conjectures*.
- 693 Fritts, H. C. (1976), *Tree Rings and Climate*, Academic Press, New York.
- 694 Gagen, M., D. McCarroll, N. J. Loader, I. Robertson, R. Jalkanen, and K. J. Anchukaitis
695 (2007), Exorcising the ‘segment length curse’: summer temperature reconstruction since
696 AD 1640 using non-detrended stable carbon isotope ratios from pine trees in northern
697 Finland, *The Holocene*, *17*(4), 435.
- 698 Gindl, W., M. Grabner, and R. Wimmer (2000), The influence of temperature on latewood
699 lignin content in treeline Norway spruce compared with maximum density and ring
700 width, *Trees*, *14*(7), 409–414, doi:10.1007/s004680000057.
- 701 Grattan, J., and D. J. Charman (1994), Non-climatic factors and the environmental im-
702 pact of volcanic volatiles: implications of the Laki fissure eruption of AD 1783, *The*
703 *Holocene*, *4*(1), 101–106.
- 704 Grattan, J., and F. Pyatt (1994), Acid damage to vegetation following the Laki fissure
705 eruption in 1783—an historical review, *Science of the Total Environment*, *151*(3), 241–
706 247.
- 707 Grattan, J., and F. Pyatt (1999), Volcanic eruptions dry fogs and the European palaeoen-
708 vironmental record: localised phenomena or hemispheric impacts?, *Global and Planetary*
709 *Change*, *21*(1-3), 173–179.
- 710 Grattan, J., and J. Sadler (1999), Regional warming of the lower atmosphere in the wake
711 of volcanic eruptions: the role of the Laki fissure eruption in the hot summer of 1783,

- 712 *Geological Society, London, Special Publications, 161*(1), 161–171.
- 713 Grattan, J., M. Durand, and S. Taylor (2003), Illness and elevated human mortality in
714 Europe coincident with the Laki Fissure eruption, *Geological Society, London, Special*
715 *Publications, 213*(1), 401–414, doi:10.1144/GSL.SP.2003.213.01.24.
- 716 Gu, L., D. D. Baldocchi, S. C. Wofsy, J. W. Munger, J. J. Michalsky, S. P. Urbanski, and
717 T. A. Boden (2003), Response of a deciduous forest to the Mount Pinatubo eruption:
718 Enhanced photosynthesis, *Science, 299*(5615), 2035–2038.
- 719 Gudmundsson, M. T., T. Thordarson, Á. Höskuldsson, G. Larsen, H. Björnsson, F. J.
720 Prata, B. Oddsson, E. Magnússon, T. Högnadóttir, G. N. Petersen, et al. (2012), Ash
721 generation and distribution from the April-May 2010 eruption of Eyjafjallajökull, Ice-
722 land, *Scientific reports, 2*(1), 1–12.
- 723 Guillet, S., C. Corona, M. Stoffel, M. Khodri, F. Lavigne, P. Ortega, N. Eckert, P. D.
724 Sielenou, V. Daux, O. V. C. (Sidorova), N. Davi, J.-L. Edouard, Y. Zhang, B. H. Luck-
725 man, V. S. Myglan, J. Guiot, M. Beniston, V. Masson-Delmotte, and C. Oppenheimer
726 (2017), Climate response to the Samalas volcanic eruption in 1257 revealed by proxy
727 records, *Nature Geoscience, 10*(2), 123–128, doi:10.1038/ngeo2875.
- 728 Gunnarson, B. E., H. W. Linderholm, and A. Moberg (2011), Improving a tree-ring
729 reconstruction from west-central Scandinavia: 900 years of warm-season temperatures,
730 *Climate Dynamics, 36*(1-2), 97–108.
- 731 Gärtner, H., and F. Schweingruber (2013), *Microscopic Preparation Techniques for Plant*
732 *Stem Analysis*, vol. 34, 83 pp., Remagen: Kessel Publishing House.
- 733 Hakim, G. J., J. Emile-Geay, E. J. Steig, D. Noone, D. M. Anderson, R. Tardif, N. Steiger,
734 and W. A. Perkins (2016), The last millennium climate reanalysis project: Framework

- 735 and first results, *Journal of Geophysical Research: Atmospheres*, *121*(12), 6745–6764.
- 736 Hansell, A., and C. Oppenheimer (2004), Health hazards from volcanic gases: a systematic
737 literature review, *Archives of Environmental Health: An International Journal*, *59*(12),
738 628–639.
- 739 Hartl, C., S. S. George, O. Konter, L. Harr, D. Scholz, A. Kirchhefer, and J. Esper (2019),
740 Warfare dendrochronology: Trees witness the deployment of the German battleship
741 Tirpitz in Norway, *Anthropocene*, *27*, 100,212.
- 742 Hevia, A., R. Sánchez-Salguero, J. J. Camarero, A. Buras, G. Sangüesa-Barreda, J. D.
743 Galván, and E. Gutiérrez (2018), Towards a better understanding of long-term wood-
744 chemistry variations in old-growth forests: a case study on ancient *Pinus uncinata* trees
745 from the Pyrenees, *Science of the Total Environment*, *625*, 220–232.
- 746 Jones, P. D., K. R. Briffa, and F. H. Schweingruber (1995), Tree-ring evidence of the
747 widespread effects of explosive volcanic eruptions, *Geophysical Research Letters*, *22*(11),
748 1333–1336.
- 749 Knohl, A., and D. D. Baldocchi (2008), Effects of diffuse radiation on canopy gas ex-
750 change processes in a forest ecosystem, *Journal of Geophysical Research: Biogeosciences*,
751 *113*(G2).
- 752 Kozlov, V., and M. Kisternaya (2004), Architectural wooden monuments as a source
753 of information for past environmental changes in Northern Russia, *Palaeogeography*,
754 *Palaeoclimatology, Palaeoecology*, *209*(1-4), 103–111.
- 755 Kurczyńska, E. U., W. Dmuchowski, W. Włoch, and A. Bytnerowicz (1997), The influ-
756 ence of air pollutants on needles and stems of Scots pine (*Pinus sylvestris* L.) trees,
757 *Environmental pollution*, *98*(3), 325–334.

- 758 Laufeld, S. (1994), The Lakagíggar 1783–84 eruption and its environmental impact in the
759 Nordic countries, *GFF*, *116*(4), 211–214, doi:10.1080/11035899409546185.
- 760 Lawrimore, J. H., M. J. Menne, B. E. Gleason, C. N. Williams, D. B. Wuertz, R. S.
761 Vose, and J. Rennie (2011), An overview of the Global Historical Climatology Net-
762 work monthly mean temperature data set, version 3, *Journal of Geophysical Research:*
763 *Atmospheres*, *116*(D19).
- 764 Leavitt, S. W., and A. Long (1982), Evidence for $^{13}\text{C}/^{12}\text{C}$ fractionation between tree
765 leaves and wood, *Nature*, *298*(5876), 742–744.
- 766 Liang, W., I. Heinrich, S. Simard, G. Helle, I. D. Liñán, and T. Heinken (2013), Climate
767 signals derived from cell anatomy of Scots pine in NE Germany, *Tree physiology*, *33*(8),
768 833–844.
- 769 Linderholm, H. W., and B. E. Gunnarson (2019), Were medieval warm-season tempera-
770 tures in Jämtland, central Scandinavian Mountains, lower than previously estimated?,
771 *Dendrochronologia*, *57*, 125,607, doi:https://doi.org/10.1016/j.dendro.2019.125607.
- 772 Loader, N., G. Young, H. Grudd, and D. McCarroll (2013), Stable carbon isotopes from
773 Torneträsk, northern Sweden provide a millennial length reconstruction of summer sun-
774 shine and its relationship to Arctic circulation, *Quaternary Science Reviews*, *62*, 97–113.
- 775 Lükewille, A., and A. Semb (1997), Deposition in Norwegian mountain areas, *NILU OR*.
- 776 Luterbacher, J., D. Dietrich, E. Xoplaki, M. Grosjean, and H. Wanner (2004), European
777 seasonal and annual temperature variability, trends, and extremes since 1500, *Science*,
778 *303*, 1499–1503.
- 779 Luterbacher, J., J. P. Werner, J. E. Smerdon, L. Fernández-Donado, F. González-Rouco,
780 D. Barriopedro, F. C. Ljungqvist, U. Büntgen, E. Zorita, S. Wagner, et al. (2016),

- 781 European summer temperatures since Roman times, *Environmental research letters*,
782 *11*(2), 024,001.
- 783 Martin, B., A. Bytnerowicz, and Y. R. Thorstenson (1988), Effects of air pollutants on
784 the composition of stable carbon isotopes, $\delta^{13}\text{C}$, of leaves and wood, and on leaf injury,
785 *Plant Physiology*, *88*(1), 218–223.
- 786 Mathias, J. M., and R. B. Thomas (2018), Disentangling the effects of acidic air pollution,
787 atmospheric CO_2 , and climate change on recent growth of red spruce trees in the Central
788 Appalachian Mountains, *Global change biology*, *24*(9), 3938–3953.
- 789 Matisons, R., H. Gärtner, D. Elferts, A. Kārklīņa, A. Adamovičs, and Ā. Jansons (2020),
790 Occurrence of ‘blue’ and ‘frost’ rings reveal frost sensitivity of eastern Baltic provenances
791 of Scots pine, *Forest Ecology and Management*, *457*, 117,729.
- 792 Mayer, K., M. Grabner, S. Rosner, M. Felhofer, and N. Gierlinger (2020), A synoptic view
793 on intra-annual density fluctuations in *Abies alba*, *Dendrochronologia*, *64*, 125,781.
- 794 Menne, M. J., C. N. Williams, B. E. Gleason, J. J. Rennie, and J. H. Lawrimore (2018),
795 The Global Historical Climatology Network monthly temperature dataset, version 4,
796 *Journal of Climate*, *31*(24), 9835–9854.
- 797 Mercado, L. M., N. Bellouin, S. Sitch, O. Boucher, C. Huntingford, M. Wild, and P. M.
798 Cox (2009), Impact of changes in diffuse radiation on the global land carbon sink,
799 *Nature*, *458*(7241), 1014–1017.
- 800 Moberg, A., H. Alexandersson, H. Bergström, and P. D. Jones (2003), Were southern
801 Swedish summer temperatures before 1860 as warm as measured?, *International Journal*
802 *of Climatology*, *23*(12), 1495–1521, doi:10.1002/joc.945.

- 803 Moberg, Anders (2020), Stockholm Historical Weather Observa-
804 tions — Daily mean air temperatures since 1756, doi:10.17043/
805 STOCKHOLM-HISTORICAL-TEMPS-DAILY-2.
- 806 Morino, K., R. L. Minor, G. A. Barron-Gafford, P. M. Brown, and M. K. Hughes (2021),
807 Bimodal cambial activity and false-ring formation in conifers under a monsoon climate,
808 *Tree Physiology*, doi:10.1093/treephys/tpab045.
- 809 Myśkow, E., M. Błaś, M. Sobik, M. Godek, and P. Owczarek (2019), The effect of pollutant
810 fog deposition on the wood anatomy of subalpine Norway spruce, *European journal of*
811 *forest research*, 138(2), 187–201.
- 812 Oman, L., A. Robock, G. L. Stenchikov, T. Thordarson, D. Koch, D. T. Shindell, and
813 C. C. Gao (2006), Modeling the distribution of the volcanic aerosol cloud from the
814 1783-1784 Laki eruption, *J. Geophys. Res. - Atmospheres*, 111(D12).
- 815 Oppenheimer, C. (2015), Eruption politics, *Nature Geoscience*, 8(4), 244–245.
- 816 Oppenheimer, C., A. Orchard, M. Stoffel, T. P. Newfield, S. Guillet, C. Corona, M. Sigl,
817 N. Di Cosmo, and U. Büntgen (2018), The Eldgjá eruption: timing, long-range impacts
818 and influence on the Christianisation of Iceland, *Climatic Change*, 147(3), 369–381.
- 819 Pearson, C., S. W. Manning, M. Coleman, and K. Jarvis (2005), Can tree-ring chemistry
820 reveal absolute dates for past volcanic eruptions?, *Journal of Archaeological Science*,
821 32(8), 1265–1274.
- 822 Pearson, C., M. Salzer, L. Wacker, P. Brewer, A. Sookdeo, and P. Kuniholm (2020),
823 Securing timelines in the ancient Mediterranean using multiproxy annual tree-ring data,
824 *Proceedings of the National Academy of Sciences*, 117(15), 8410–8415.

- 825 Pearson, C. L., S. W. Manning, M. Coleman, and K. Jarvis (2006), A dendrochemical
826 study of *Pinus sylvestris* from Siljansfors Experimental Forest, central Sweden, *Applied*
827 *Geochemistry*, *21*(10), 1681–1691.
- 828 Pearson, C. L., D. Dale, P. Brewer, M. Salzer, J. Lipton, and S. Manning (2009), Den-
829 drochemistry of White Mountain bristlecone pines: An investigation via Synchrotron
830 Radiation Scanning X-Ray Fluorescence Microscopy, *Journal of Geophysical Research:*
831 *Biogeosciences*, *114*(G1).
- 832 Piermattei, A., A. Crivellaro, M. Carrer, and C. Urbinati (2015), The “blue ring”:
833 anatomy and formation hypothesis of a new tree-ring anomaly in conifers, *Trees*, *29*(2),
834 613–620.
- 835 Piermattei, A., A. Crivellaro, P. J. Krusic, J. Esper, P. Vitek, C. Oppenheimer, M. Fel-
836 hofer, N. Gierlinger, F. Reinig, O. Urban, et al. (2020), A millennium-long ‘Blue Ring’
837 chronology from the Spanish Pyrenees reveals severe ephemeral summer cooling after
838 volcanic eruptions, *Environmental Research Letters*, *15*(12), 124,016.
- 839 Prendin, A. L., G. Petit, M. Carrer, P. Fonti, J. Björklund, and G. von Arx (2017), New
840 research perspectives from a novel approach to quantify tracheid wall thickness, *Tree*
841 *Physiology*, *37*(7), 976–983, doi:10.1093/treephys/tpx037.
- 842 R Core Team (2019), *R: A Language and Environment for Statistical Computing*, R Foun-
843 dation for Statistical Computing, Vienna, Austria.
- 844 Rathgeber, C. B. K., H. E. Cuny, and P. Fonti (2016), Biological basis of tree-ring forma-
845 tion: A crash course, *Frontiers in Plant Science*, *7*, doi:10.3389/fpls.2016.00734.
- 846 Rayback, S. A., S. Belmecheri, M. H. Gagen, A. Lini, R. Gregory, and C. Jenkins (2020),
847 North American temperate conifer (*Tsuga canadensis*) reveals a complex physiological

- 848 response to climatic and anthropogenic stressors, *New Phytologist*, *228*(6), 1781–1795.
- 849 Robock, A. (2000), Volcanic eruptions and climate, *Review of Geophysics*, *38*, 191–219.
- 850 Robock, A. (2005), Cooling following large volcanic eruptions corrected for the effect of
851 diffuse radiation on tree rings, *Geophys. Res. Lett.*, *32*(L06702), L06702, doi:10.1029/
852 2004GL022116.
- 853 Rocha, E., B. Gunnarson, M. E. Kylander, A. Augustsson, A. Rindby, and S. Holzkämper
854 (2020), Testing the applicability of dendrochemistry using X-ray fluorescence to trace
855 environmental contamination at a glassworks site, *Science of the Total Environment*,
856 *720*, 137,429.
- 857 Rohde, R. A., and Z. Hausfather (2020), The Berkeley Earth land/ocean temperature
858 record, *Earth System Science Data*, *12*(4), 3469–3479.
- 859 Schmidt, A. (2015), Volcanic gas and aerosol hazards from a future Laki-type eruption in
860 Iceland, in *Volcanic Hazards, Risks and Disasters*, pp. 377–397, Elsevier.
- 861 Schmidt, A., B. Ostro, K. S. Carslaw, M. Wilson, T. Thordarson, G. W. Mann, and A. J.
862 Simmons (2011), Excess mortality in Europe following a future Laki-style Icelandic
863 eruption, *Proceedings of the National Academy of Sciences*, *108*(38), 15,710–15,715.
- 864 Schove, D. J. (1954), Summer temperatures and tree-rings in North-Scandinavia AD 1461–
865 1950, *Geografiska Annaler*, *36*(1-2), 40–80.
- 866 Seftigen, K., H. W. Linderholm, N. J. Loader, Y. Liu, and G. H. Young (2011), The influ-
867 ence of climate on $^{13}\text{C}/^{12}\text{C}$ and $^{18}\text{O}/^{16}\text{O}$ ratios in tree ring cellulose of *Pinus sylvestris*
868 L. growing in the central Scandinavian Mountains, *Chemical Geology*, *286*(3-4), 84–93.
- 869 Sheppard, P. R., M. H. Ort, K. C. Anderson, M. A. Clynne, and E. M. May (2009),
870 Multiple dendrochronological responses to the eruption of Cinder Cone, Lassen volcanic

- 871 National Park, California, *Dendrochronologia*, *27*(3), 213–221.
- 872 Sigl, M., M. Winstrup, J. R. McConnell, K. C. Welten, G. Plunkett, F. Ludlow,
873 U. Büntgen, M. Caffee, N. Chellman, D. Dahl-Jensen, H. Fischer, S. Kipfstuhl, C. Ko-
874 stick, O. J. Maselli, F. Mekhaldi, R. Mulvaney, R. Muscheler, D. R. Pasteris, J. R.
875 Pilcher, M. Salzer, S. Schüpbach, J. P. Steffensen, B. M. Vinther, and T. E. Woodruff
876 (2015), Timing and climate forcing of volcanic eruptions for the past 2,500 years, *Nature*,
877 *523*(7562), 543–549, doi:10.1038/nature14565.
- 878 Smith, K. T., J. C. Balouet, and G. Oudijk (2008), Elemental line scanning of an increment
879 core using EDXRF: From fundamental research to environmental forensics applications,
880 *Dendrochronologia*, *26*(3), 157–163.
- 881 Sonnek, K. M., T. Mårtensson, E. Veibäck, P. Tunved, H. Grahn, P. von Schoenberg,
882 N. Brännström, and A. Bucht (2017), The impacts of a Laki-like eruption on the present
883 Swedish society, *Natural Hazards*, *88*(3), 1565–1590.
- 884 Stothers, R. B. (1996), The great dry fog of 1783, *Climatic change*, *32*(1), 79–89.
- 885 Szeicz, J. M. (1996), White spruce light rings in northwestern Canada, *Arctic and Alpine*
886 *Research*, *28*(2), 184–189, doi:10.1080/00040851.1996.12003164.
- 887 Tardif, R., G. J. Hakim, W. A. Perkins, K. A. Horlick, M. P. Erb, J. Emile-Geay, D. M. An-
888 derson, E. J. Steig, and D. Noone (2019), Last Millennium Reanalysis with an expanded
889 proxy database and seasonal proxy modeling, *Climate of the Past*, *15*(4), 1251–1273,
890 doi:10.5194/cp-15-1251-2019.
- 891 Thomas, R. B., S. E. Spal, K. R. Smith, and J. B. Nippert (2013), Evidence of recovery
892 of *Juniperus virginiana* trees from sulfur pollution after the Clean Air Act, *Proceedings*
893 *of the National Academy of Sciences*, *110*(38), 15,319–15,324.

- 894 Thorarinsson, S. (1981), Greetings from Iceland: Ash-falls and volcanic aerosols in Scan-
895 dinavia, *Geografiska Annaler: Series A, Physical Geography*, 63(3-4), 109–118.
- 896 Thordarson, T., and G. Larsen (2007), Volcanism in Iceland in historical time: Volcano
897 types, eruption styles and eruptive history, *Journal of Geodynamics*, 43(1), 118–152.
- 898 Thordarson, T., and S. Self (1993), The Laki (Skaftár fires) and Grímsvötn eruptions in
899 1783–1785, *Bulletin of Volcanology*, 55(4), 233–263.
- 900 Thordarson, T., and S. Self (2003), Atmospheric and environmental effects of the
901 1783–1784 Laki eruption: A review and reassessment, *Journal of Geophysical Research*,
902 108(D1), doi:10.1029/2001jd002042.
- 903 Timmreck, C. (2012), Modeling the climatic effects of large explosive volcanic eruptions,
904 *Wiley Interdisciplinary Reviews: Climate Change*, 3(6), 545–564, doi:10.1002/wcc.192.
- 905 Tingley, M. P., and P. Huybers (2013), Recent temperature extremes at high northern
906 latitudes unprecedented in the past 600 years, *Nature*, 496(7444), 201–205, doi:10.1038/
907 nature11969.
- 908 Tingley, M. P., A. R. Stine, and P. Huybers (2014), Temperature reconstructions from
909 tree-ring densities overestimate volcanic cooling, *Geophysical Research Letters*, 41(22),
910 7838–7845.
- 911 Vaganov, E. (1990), The tracheidogram method in tree-ring analysis and its application,
912 in *Methods of dendrochronology: applications in the environmental sciences*, edited by
913 E. Cook and L. Kairiūkštis, pp. 63–75, Kluwer Academic Publishers, Netherlands.
- 914 Vaganov, E. A., M. K. Hughes, and A. V. Shashkin (2006), *Growth dynamics of conifer*
915 *tree rings: images of past and future environments*, vol. 183, Springer Science & Business
916 Media.

- 917 Vejputsková, M., T. Čihák, A. Samusevich, A. Zeidler, R. Novotný, and V. Šrámek (2017),
918 Interactive effect of extreme climatic event and pollution load on growth and wood
919 anatomy of spruce, *Trees*, *31*(2), 575–586.
- 920 von Arx, G., and M. Carrer (2014), ROXAS – a new tool to build centuries-long
921 tracheid-lumen chronologies in conifers, *Dendrochronologia*, *32*(3), 290–293, doi:10.
922 1016/j.dendro.2013.12.001.
- 923 von Arx, G., A. Crivellaro, A. L. Prendin, K. Čufar, and M. Carrer (2016), Quantitative
924 wood anatomy—practical guidelines, *Frontiers in Plant Science*, *7*, doi:10.3389/fpls.
925 2016.00781.
- 926 Walmsley, J., N. Urquizo, R. Schemenauer, and H. Bridgman (1970), Modelling of acid
927 deposition in high-elevation fog, *WIT Transactions on Ecology and the Environment*,
928 *14*.
- 929 Watanabe, Y., and Y. Ohno (2020), Severe insect defoliation at different timing affects
930 cell wall formation of tracheids in secondary xylem of *Larix kaempferi*, *Trees*, pp. 1–11.
- 931 Watmough, S. A. (1997), An evaluation of the use of dendrochemical analyses in environ-
932 mental monitoring, *Environmental Reviews*, *5*(3-4), 181–201.
- 933 Watt, S. F., D. M. Pyle, T. A. Mather, J. A. Day, and A. Aiuppa (2007), The use of
934 tree-rings and foliage as an archive of volcanogenic cation deposition, *Environmental*
935 *Pollution*, *148*(1), 48–61.
- 936 Wilson, R., K. Anchukaitis, K. R. Briffa, U. Büntgen, E. Cook, R. D’Arrigo, N. Davi,
937 J. Esper, D. Frank, B. Gunnarson, G. Hegerl, S. Helama, S. Klesse, P. J. Krusic, H. W.
938 Linderholm, V. Myglan, T. J. Osborn, M. Rydval, L. Schneider, A. Schurer, G. Wiles,
939 P. Zhang, and E. Zorita (2016), Last millennium northern hemisphere summer tem-

- 940 peratures from tree rings: Part I: The long term context, *Quaternary Science Reviews*,
941 *134*, 1–18, doi:10.1016/j.quascirev.2015.12.005.
- 942 Wimmer, R. (2002), Wood anatomical features in tree-rings as indicators of environmental
943 change, *Dendrochronologia*, *20*(1-2), 21–36.
- 944 Wimmer, R., G. Strumia, and F. Holawe (2000), Use of false rings in Austrian pine to
945 reconstruct early growing season precipitation, *Canadian Journal of Forest Research*,
946 *30*(11), 1691–1697.
- 947 Witham, C. S., and C. Oppenheimer (2004), Mortality in England during the 1783–4 Laki
948 Craters eruption, *Bulletin of Volcanology*, *67*(1), 15–26.
- 949 Young, G. H., D. McCarroll, N. J. Loader, M. H. Gagen, A. J. Kirchhefer, and J. C.
950 Demmler (2012), Changes in atmospheric circulation and the Arctic Oscillation pre-
951 served within a millennial length reconstruction of summer cloud cover from northern
952 Fennoscandia, *Climate dynamics*, *39*(1), 495–507.
- 953 Zambri, B., A. Robock, M. J. Mills, and A. Schmidt (2019a), Modeling the 1783–1784
954 Laki Eruption in Iceland: 2. Climate Impacts, *Journal of Geophysical Research: Atmo-*
955 *spheres*, *124*(13), 6770–6790, doi:10.1029/2018jd029554.
- 956 Zambri, B., A. Robock, M. J. Mills, and A. Schmidt (2019b), Modeling the 1783–1784
957 Laki Eruption in Iceland: 1. Aerosol Evolution and Global Stratospheric Circulation
958 Impacts, *Journal of Geophysical Research: Atmospheres*, *124*(13), 6750–6769, doi:10.
959 1029/2018jd029553.
- 960 Zhang, P., H. W. Linderholm, B. E. Gunnarson, J. Björklund, and D. Chen (2016), 1200
961 years of warm-season temperature variability in central Scandinavia inferred from tree-
962 ring density, *Climate of the Past*, *12*(6), 1297–1312, doi:10.5194/cp-12-1297-2016.

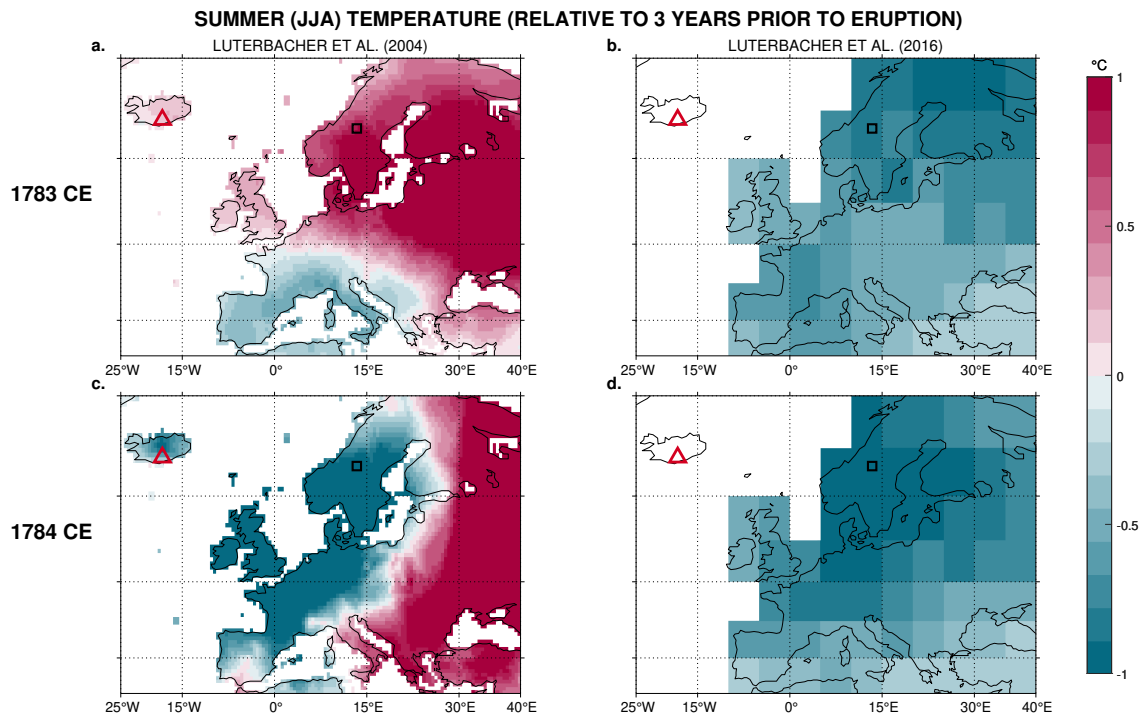


Figure 1. Proxy reconstructed summer (June through August) mean temperature anomalies in 1783 CE from (a), *Luterbacher et al.* [2004] and (b), *Luterbacher et al.* [2016], and in 1784 CE from (c), *Luterbacher et al.* [2004] and (d), *Luterbacher et al.* [2016], relative to the mean temperature of the 3 years prior to the Laki eruption. The red triangle marks the location of the Laki volcano and the black square marks the location of the Jämtland study site. The positive temperature anomaly in (a) is dominated by the use of historical, documentary, and early instrumental data. (b) is created mostly from tree-ring proxy data, including MXD at the Jämtland site [*Gunnarson et al.*, 2011]. Other temperature field reconstructions using a wide range of proxy observations and statistical methods also show cooling over Northern Europe in 1783 (see Figure 1 in *Edwards et al.*

D R A F T
 [2021]) [Tingley and Huybers, 2013; Anchukaitis et al., 2017; Guillet et al., 2017; Tardif et al., 2019, e.g.].
 November 9, 2021, 8:01pm
 D R A F T

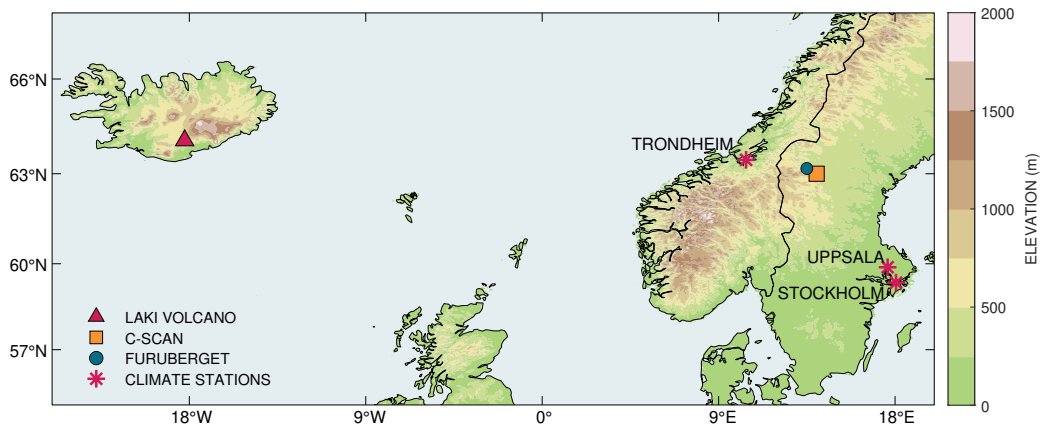


Figure 2. Map of locations relevant to this study. C-Scan (orange square) is the general area of the Jämtland (Sweden) sampling sites where the *P. sylvestris* samples used in this study were collected. Furuberget (blue circle) is the sampling site from *Seftigen et al.* [2011] where tree-ring carbon isotope data covering the eruption period are available. The mapped location of the Trondheim climate station (pink asterisk) is the approximate average location between the Trondheim/Tyholt and Trondheim/Vaernes stations.

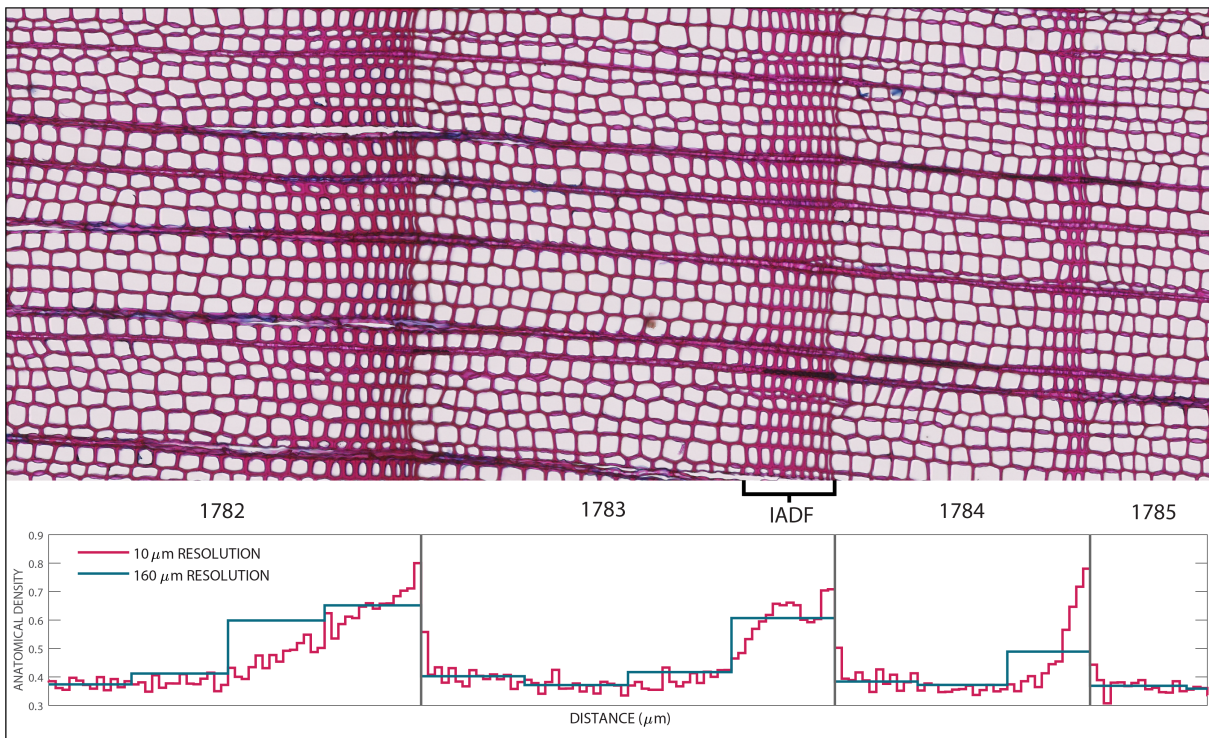


Figure 3. Example micrograph of Scots pine sample Hror001 from Jämtland, stained with safranin. An intra-annual density fluctuation (IADF) can be seen in the 1783 ring. Earlywood to latewood growth is shown going from left to right. Raw values of intra-annual measurements of anatomical density taken at 10 μm and 160 μm resolution are plotted at their approximate location within each annual ring.

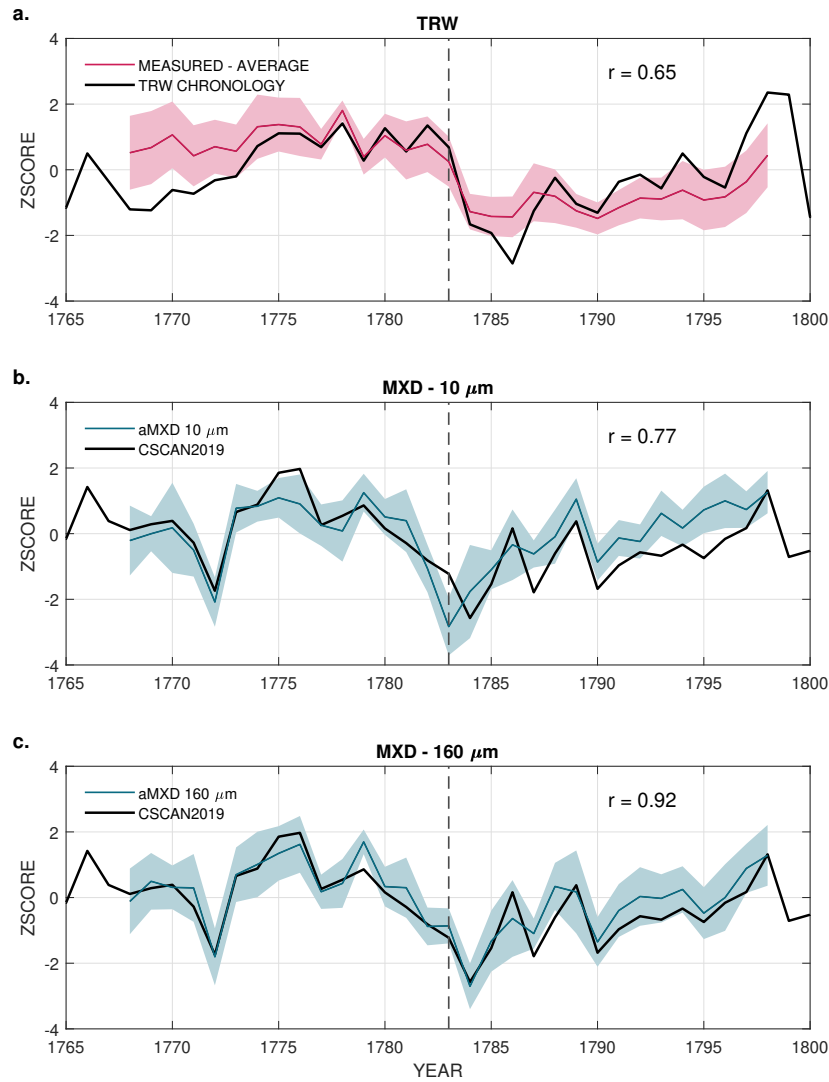


Figure 4. (a) Full sample ($N = 24$) tree-ring width (TRW) chronology (black line) and average tree-ring width of samples measured in ROXAS ($N=9$, red line). (b,c) Updated CSCAN2019 MXD chronology (black line) from *Linderholm and Gunnarson* [2019] and the anatomical MXD (aMXD) measurements (blue line) at a resolution of 10 microns (b) and 160 microns (c). Results from the Pearson correlation coefficient calculations are included in each plot. Values are normalized for comparison of the related, but different, measurements. The data in this study were analyzed over the 30-year period: 1768–1798. Shaded regions show the ± 1 standard deviation around the mean values. None of the anatomical chronologies were detrended. The aMXD10 has a lower correlation with the CSCAN2019 MXD chronology because of the drop in density in the last part of the ring that is captured by the high-resolution aMXD.

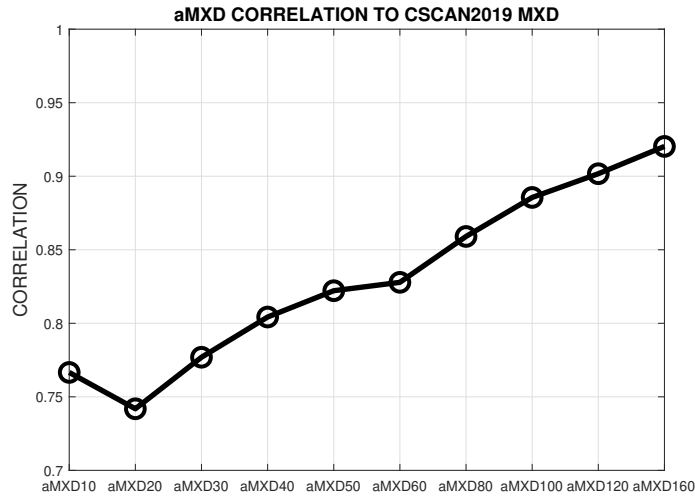


Figure 5. Results from the Pearson correlation coefficient calculations between the CSCAN2019 MXD chronology and each aMXD chronology from 1768–1798. All correlations are significant at $p < 0.001$.

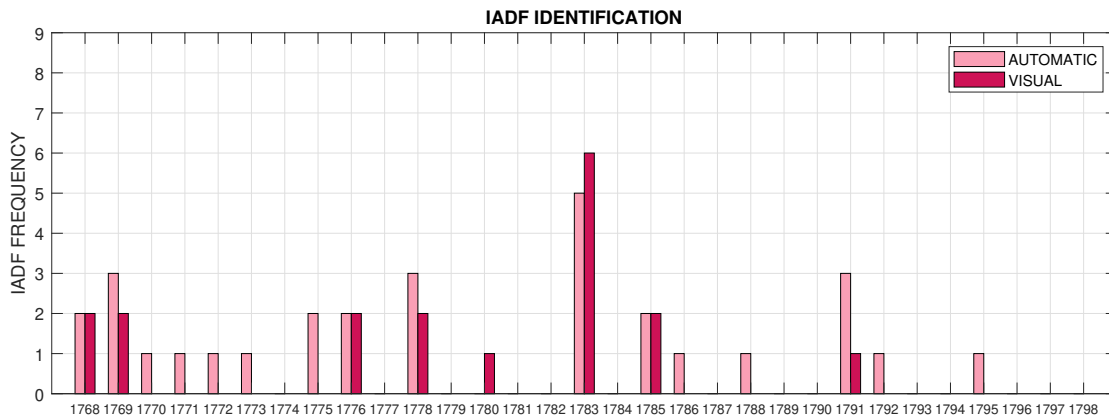


Figure 6. Intra-annual density fluctuation (IADF) frequency from 1768–1798 CE based on automatic detection (light pink) and visual identification (dark pink). Frequency is out of 9 possible trees for every year for both identification methods.

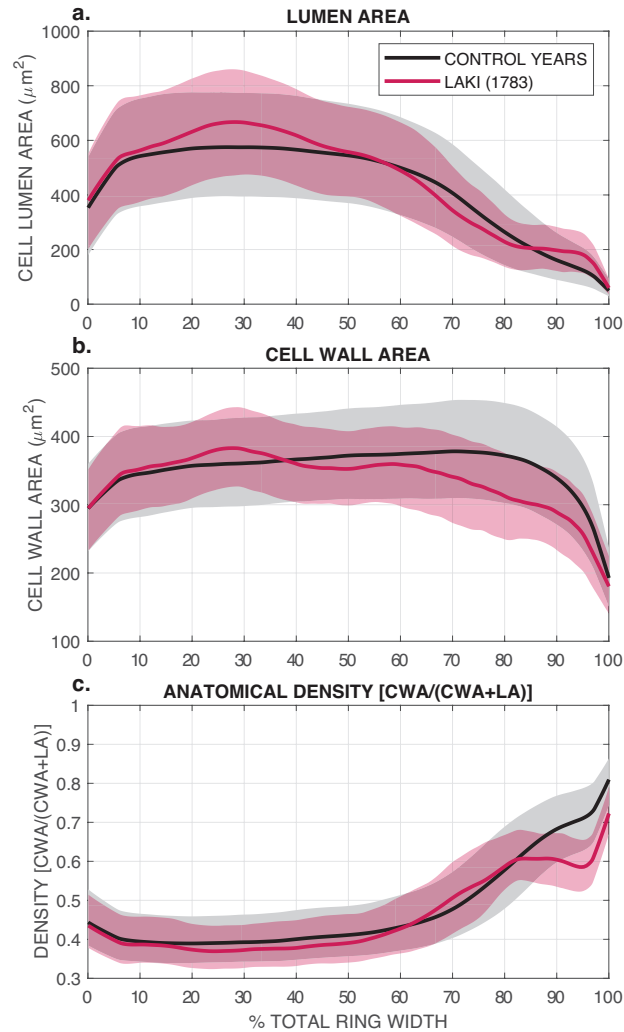


Figure 7. Lumen area, cell wall area, and anatomical density measurements plotted according to their relative position in the tree ring. The anatomical density is the ratio between the cell wall area (CWA) and the sum of cell wall area (CWA) and cell lumen area (LA). The red line is the lowest curve of all cell measurement for the 1783 year throughout the different relative positions in the ring. The red envelope represents the area between the lowest curves fit to the residuals of the original lowest curve. The black line is the lowest curve fit to all cell measurements of the control years: 15 years before and after the 1783 Laki eruption. The grey envelope represents the area between the lowest curves fit to the residuals of the original lowest curve for the control years.

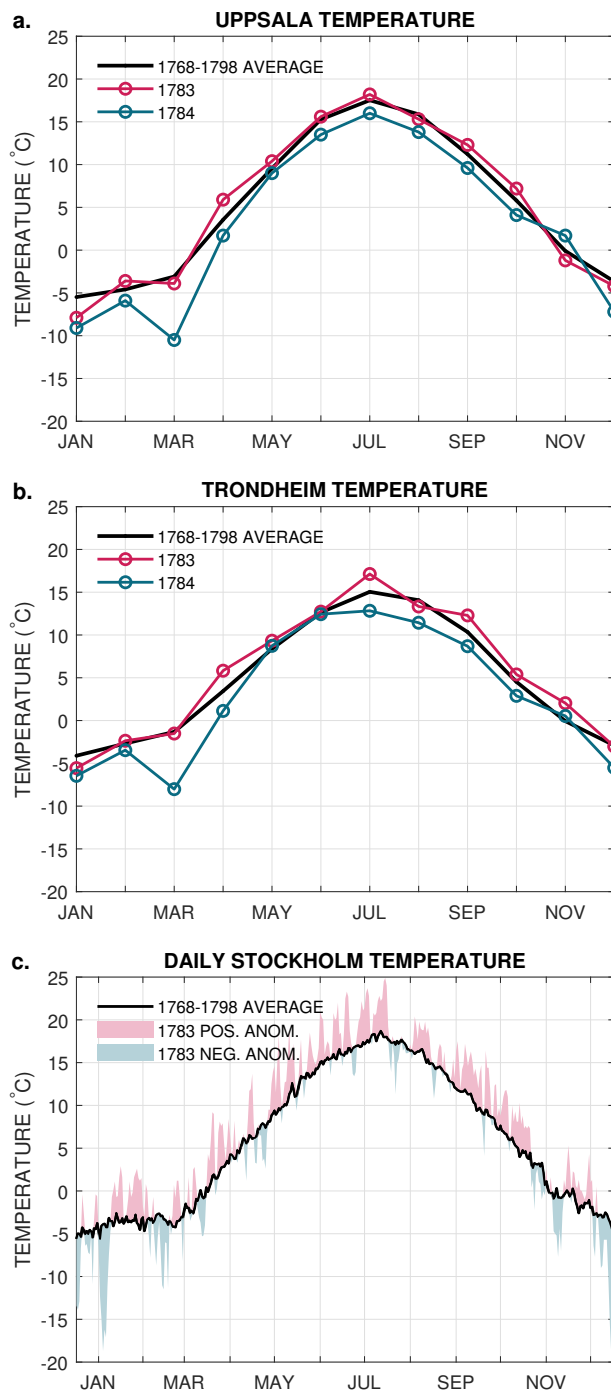


Figure 8. Historical monthly temperature data from the Uppsala (a) and the average Trondheim (b) climate stations. Temperature for 1783 CE (red), 1784 CE (blue), and the average temperature over the 1768–1798 CE period (black) are plotted (a,b). Daily temperature data from the Stockholm climate station (c): positive 1783 CE temperature anomalies over the 1768–198 CE average (black) are plotted with red, while negative 1783 CE temperature anomalies are plotted with blue. X-axis tick marks in panel c mark the halfway point of each month.

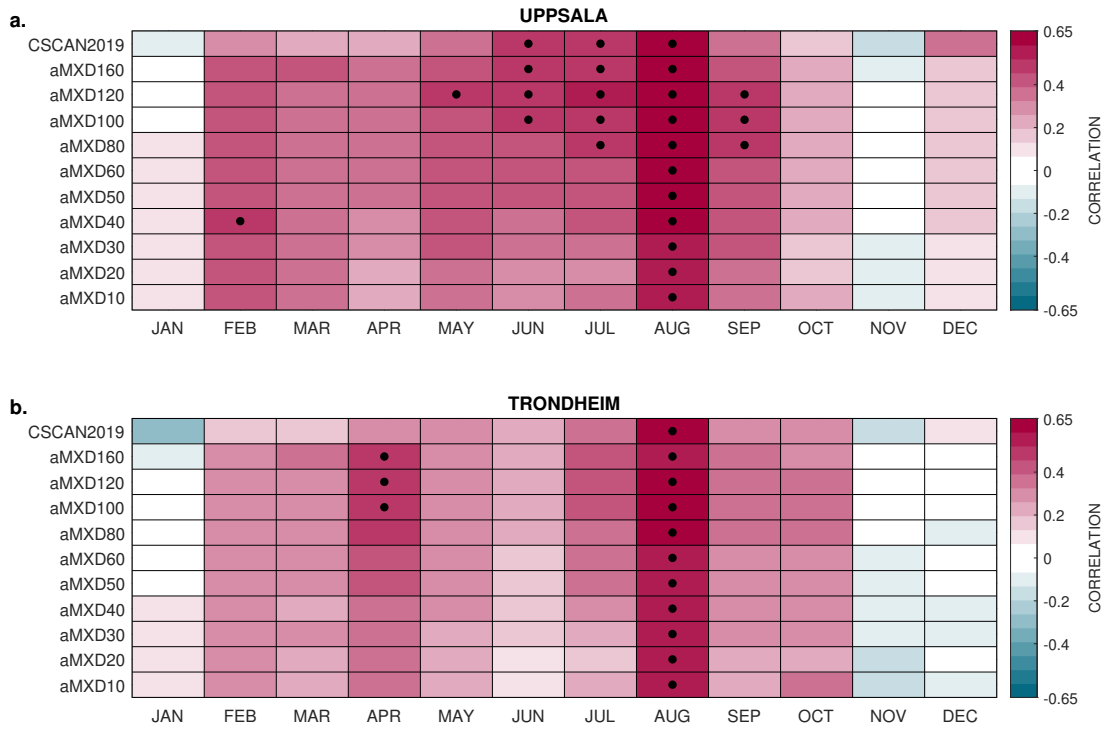


Figure 9. Results from the Pearson correlation coefficient calculations between the monthly data at Uppsala (a) and Trondheim (b), and the multiple resolution aMXD and CSCAN2019 MXD chronologies from 1768–1798 CE. Significant correlations ($\alpha = 0.01$) are indicated with a dot.

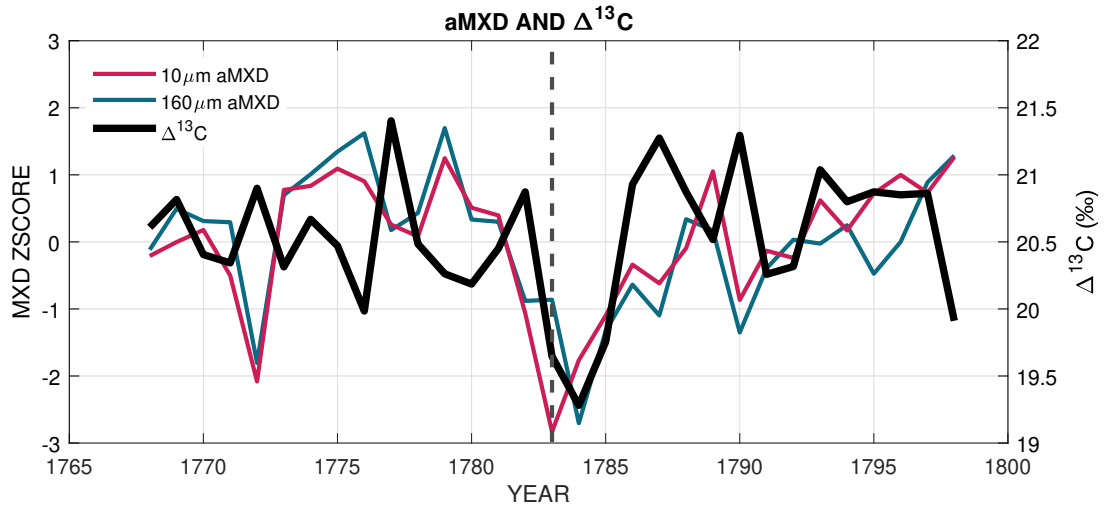


Figure 10. Time series of $\Delta^{13}\text{C}$ (black) converted from [Seftigen *et al.*, 2011] and aMXD chronologies at the 10 μm resolution (red) and at the 160 μm resolution (blue). aMXD chronologies are normalized.

Chronology	1768–1798 <i>r</i>	1768–1798 <i>p</i> -value	1783–1785 excluded <i>r</i>	1783–1785 excluded <i>p</i> -values
aMXD10	0.18	0.32	-0.43	0.02
aMXD20	0.23	0.21	-0.35	0.07
aMXD30	0.22	0.23	-0.38	0.05
aMXD40	0.17	0.36	-0.44	0.02
aMXD50	0.17	0.37	-0.46	0.01
aMXD60	0.15	0.43	-0.48	<0.01
aMXD80	0.12	0.53	-0.52	<0.01
aMXD100	0.08	0.69	-0.56	<0.01
aMXD120	0.05	0.80	-0.59	<0.01
aMXD160	0.02	0.91	-0.62	<0.01
CSCAN2019	-0.03	0.88	-0.60	<0.01

Table 1. Results from the Pearson correlation coefficient calculations between the $\Delta^{13}\text{C}$ series [Seftigen *et al.*, 2011] and the multiple resolution aMXD and CSCAN2019 MXD chronologies from 1768–1798, with and without excluding concurrent and post-volcanic eruption years 1783, 1784, and 1785.